iScience

CellPress
OPEN ACCESS

Article

An inducible CRISPR/Cas9 screen identifies DTX2 as a transcriptional regulator of human telomerase

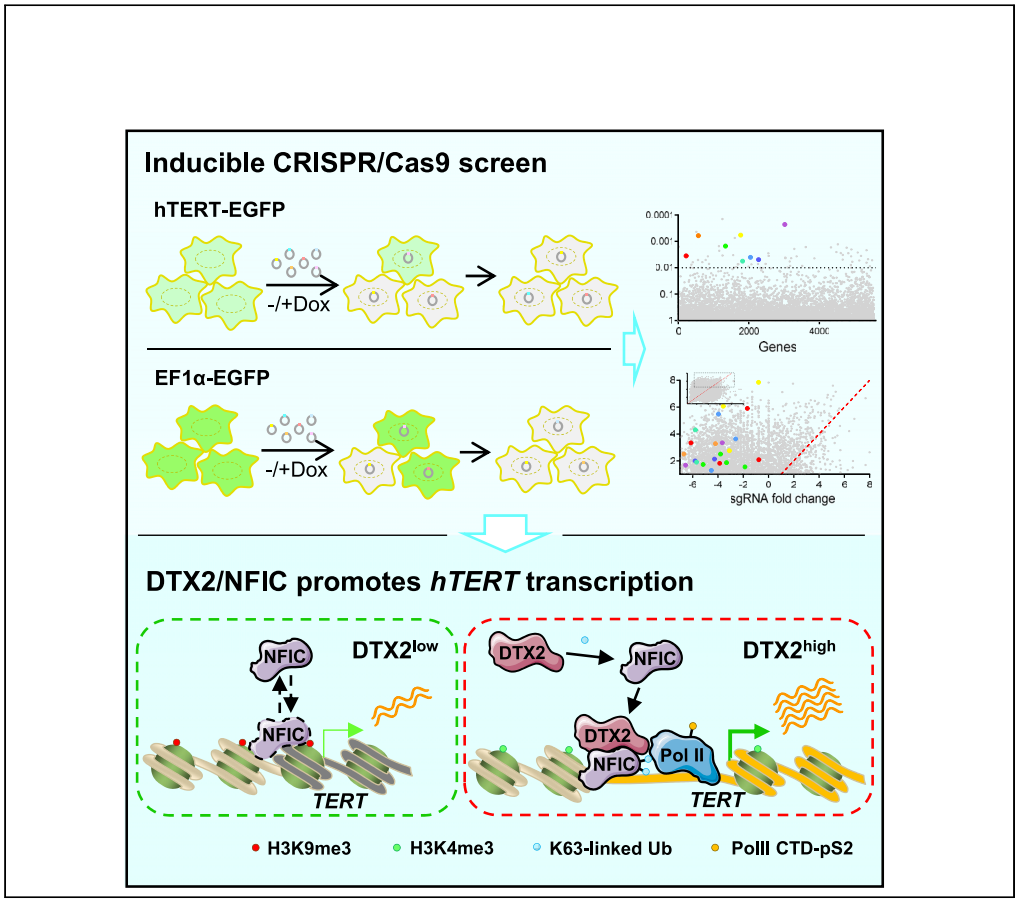

Zhifen Zhou, Yujing Li, Huimin Xu, ..., Su Wu, Wenbin Ma, Zhou Songyang

songyanz@mail.sysu.edu.cn (Z.S.)
mawenbin@mail.sysu.edu.cn (W.M.)
wusu5@mail.sysu.edu.cn (S.W.)

Highlights

An inducible CRISPR/Cas9 screen identifies regulators for *hTERT* transcription

DTX2 deficiency leads to telomere shortening and cell growth arrest

DTX2 mediates ubiquitination on NFIC, stabilizing NFIC binding on *hTERT* promoter

DTX2-NFIC functions corporately to promote *hTERT* transcription and tumorigenesis

Zhou et al., iScience *25*, 103813
February 18, 2022
https://doi.org/10.1016/j.isci.2022.103813

iScience

CellPress
OPEN ACCESS

Article

An inducible CRISPR/Cas9 screen identifies DTX2 as a transcriptional regulator of human telomerase

Zhifen Zhou,[1,2] Yujing Li,[2] Huimin Xu,[2] Xiaowei Xie,[2] Zibin He,[2] Song Lin,[2] Ruofei Li,[2] Shouheng Jin,[2] Jun Cui,[2] Hai Hu,[1] Feng Liu,[2] Su Wu,[1,2,*] Wenbin Ma,[2,*] and Zhou Songyang[1,2,3,4,*]

SUMMARY

Most tumor cells reactivate telomerase to ensure unlimited proliferation, whereas the expression of human telomerase reverse transcriptase (*hTERT*) is tightly regulated and rate-limiting for telomerase activity maintenance. Several general transcription factors (TFs) have been found in regulating *hTERT* transcription; however, a systematic study is lacking. Here we performed an inducible CRISPR/Cas9 KO screen using an *hTERT* core promoter-driven reporter. We identified numerous positive regulators including an E3 ligase DTX2. In telomerase-positive cancer cells, DTX2 depletion downregulated *hTERT* transcription and telomerase activity, contributing to progressive telomere shortening, growth arrest, and increased apoptosis. Utilizing BioID, we characterized multiple TFs as DTX2 proximal proteins, among which NFIC functioned corporately with DTX2 in promoting *hTERT* transcription. Further analysis demonstrated that DTX2 mediated K63-linked ubiquitination of NFIC, which facilitated NFIC binding to the *hTERT* promoter and enhanced *hTERT* expression. These findings highlight a new *hTERT* regulatory pathway that may be exploited for potential cancer therapeutics.

INTRODUCTION

Telomeres are crucial to maintaining the natural ends of linear chromosomes (Blackburn et al., 2015). Telomere DNA undergoes progressive shortening with each cell division (Harley et al., 1990; Victorelli and Passos, 2017). Critically short telomeres can trigger growth arrest and cell death (Hayashi et al., 2015; Saretzki et al., 1999), and cells that escape from such crisis may eventually lead to tumorigenesis (Maciejowski and de Lange, 2017; Wright et al., 1989). Human telomeres consist of TTAGGG tandem repeats that are elongated by the telomerase complex, with the reverse transcriptase hTERT and RNA component hTR/hTERC as its core components (Blackburn and Collins, 2011; Wang et al., 2019). Telomerase activity appears undetectable in most normal human somatic cells but present in ~90% of cancer and immortalized cells (Shay, 2013), underscoring the importance of upregulated telomerase activity in cancer development. Understanding the pathways that regulate telomerase expression and activity promises to provide valuable insight into cancer development and treatment.

Unlike hTERC, which is highly and ubiquitously expressed even in tissues with no detectable telomerase activity, hTERT expression appears suppressed in nearly all normal somatic cells (Shay, 2016; Zhang et al., 2016) and rate-limiting for maintaining cellular telomerase activity, given its positive correlation with telomerase activity (Ramlee et al., 2016; Weinrich et al., 1997). hTERT expression can be controlled at the transcriptional, posttranscriptional (e.g., alternative splicing), and posttranslational (e.g., phosphorylation) level. Transcriptionally, *hTERT* suppression in normal cells and its reactivation in cancer cells may occur through distinct but interconnected mechanisms, including regulation through transcription factors, mutations in the *hTERT* promoter, and epigenetic modifications of the *hTERT* locus (e.g., DNA methylation and histone acetylation). Low hTERT expression in human somatic cells largely attributes to the condensed heterochromatin that surrounds the *hTERT* gene (Wang et al., 2009; Zhang et al., 2016). However, in telomerase-positive tumor cells, the chromatin region near the *hTERT* transcription start site (TSS) becomes relatively open, as evidenced by the presence of DNaseI-hypersensitive sites (Wang and Zhu, 2003; Zhu et al., 2010).

Multifunctional transcription factors such as c-MYC, NF-κB, and STAT3 can upregulate *hTERT* transcription in cancer cells (Ramlee et al., 2016). Transcription factor binding appears to concentrate within 400 bps

[1]Sun Yat-sen Memorial Hospital, Sun Yat-sen University, Guangzhou 510120, China

[2]MOE Key Laboratory of Gene Function and Regulation, State Key Laboratory of Biocontrol, Guangzhou Key Laboratory of Healthy Aging Research, Institute of Healthy Aging Research, School of Life Sciences, Sun Yat-sen University, Guangzhou 510275, China

[3]Bioland Laboratory (Guangzhou Regenerative Medicine and Health Guangdong Laboratory), Guangzhou 510005, China

[4]Lead contact

*Correspondence: songyanz@mail.sysu.edu.cn (Z.S.), mawenbin@mail.sysu.edu.cn (W.M.), wusu5@mail.sysu.edu.cn (S.W.)

https://doi.org/10.1016/j.isci.2022.103813

upstream of *hTERT* TSS, which contains E-box and GC repeats and recruits factors such as Sp1/3, AP-2, USFs, and Myc family proteins (Ramlee et al., 2016). In addition, oncoproteins including HER2, Ras, and Raf are also capable of stimulating *hTERT* transcription via ETS transcription factors (Goueli and Janknecht, 2004). To date, there remains a dearth of information regarding specific positive regulators of *hTERT* transcription, and systematic studies are needed to elucidate the regulatory network that enables *hTERT* reactivation in cancer cells.

Here, we performed an inducible CRISPR/Cas9 knockout (KO) screen to identify positive regulators of *hTERT* expression, utilizing two sgRNA libraries respectively targeting nuclear genes and genes of unknown function. Our screen revealed multiple candidates that could upregulate *hTERT* expression including the E3 ubiquitin ligase DTX2. DTX2 KO in telomerase-positive cancer cells significantly reduced *hTERT* mRNA level as well as telomerase activity, resulting in progressive telomere shortening and cell growth arrest. A large-scale affinity purification screen using proximity-dependent biotin identification (BioID) further identified nuclear factor I C (NFIC) as a DTX2-associating protein. We demonstrated that DTX2 could interact with NFIC and mediate K63-linked ubiquitination of NFIC to facilitate its binding to the *hTERT* core promoter, which in turn enhanced *hTERT* transcription. Our work presents a more comprehensive list of candidate positive regulators of *hTERT* expression and highlights DTX2-mediated ubiquitination of transcription factors as a novel regulatory pathway for *hTERT* transcription and telomere maintenance.

RESULTS

An inducible CRISPR/Cas9 screen identifies positive regulators for *hTERT* transcription

To systematically search for *hTERT* transcriptional regulators, we stably expressed EGFP driven by the *hTERT* core promoter (Higashi et al., 2014) (hTERT-EGFP) in the telomerase-positive HeLa line that also expressed doxycycline (Dox)-inducible Cas9 (HeLa-iCas9) (Kim et al., 2017) (Figure 1A). HeLa-iCas9 cells expressing EF1α promoter-driven EGFP were also generated (EF1α-EGFP) to help exclude general factors regulating transcription and protein stability. $EGFP^+$ cells were enriched by fluorescence-activated cell sorting (FACS) and then transduced with two lentiviral sgRNA libraries respectively targeting 3,733 nuclear genes and 1,808 genes of unknown function (10 sgRNAs/gene) (Wang et al., 2014). Cells cultured without Dox (i.e., basal groups) served as the baseline for all subsequent analysis. Upon Dox-induced Cas9 expression, cells with specific gene KO and loss of EGFP signal were enriched by FACS as sorted groups. Cells from basal groups and sorted groups were then processed for next-generation sequencing (NGS) to calculate sgRNA abundance.

NGS analysis revealed considerable shifts and decreased clustering in sgRNA distributions following KO induction (Figure S1A). Known *hTERT* transcription factors AP-2, USF1/2, NF-κB, and STAT3 were targeted by our sgRNA libraries, but sgRNA recovery was very low for these genes in both sorted groups, likely reflecting their importance for general transcription and cell survival. Overall, 257 potential positive regulators of *hTERT* transcription were identified (Figure S1B), including epigenetic regulators involved in histone acetylation (KAT2A and KAT6A) and H3K4 methylation (MLL4). MAGeCK analysis (Li et al., 2014) revealed several genes significantly enriched in the hTERT-EGFP group (with multiple high-ranking sgRNAs), which have never been implicated in *hTERT* transcriptional regulation (Figures 1B, 1C and S1C, and Tables S1, S2). Using HEK293T-iCas9 and HeLa-iCas9 KO cell pools (Figure S1D), we verified that depletion of ASXL2, DTX2, FGF1, or FOXD3 led to decreased *hTERT* mRNA levels (Figures 1D and 1E) coupled with reduced telomerase activities (Figures S1E and S1F), supporting a role of these genes in promoting *hTERT* transcription. In particular, loss of DTX2 gave rise to a prominent effect. Given its high expression in multiple cancers (according to TCGA and GTEx (Tang et al., 2017) (Figure S1G), we hypothesized that DTX2 might facilitate tumor progression through upregulating *hTERT* transcription.

It has been shown that telomerase inhibition in cells with short telomeres can cause cell growth arrest and even apoptosis (Zhang et al., 1999). Inhibition of hTERT could induce immediate cell growth arrest by blocking them in S phase, whereas apoptosis might be induced via extra-telomeric effects on activation of p53 and p21 (Celeghin et al., 2016; Luo et al., 2009). When we knocked down *DTX2* in telomerase-positive cancer lines (e.g., HT-1080, Hs578T, and MDA-MB-231) with relatively short telomeres (Figure S1H), growth arrest and increased apoptosis were readily detectable (Figures 2A–2D and S2A–S2H). In comparison, the effect of *DTX2* knockdown in cancer lines (e.g., HeLa and DLD1) with longer telomeres was modest, although still comparable to *hTERT* knockdown (Figures S2I–S2P). Therefore, DTX2 may be

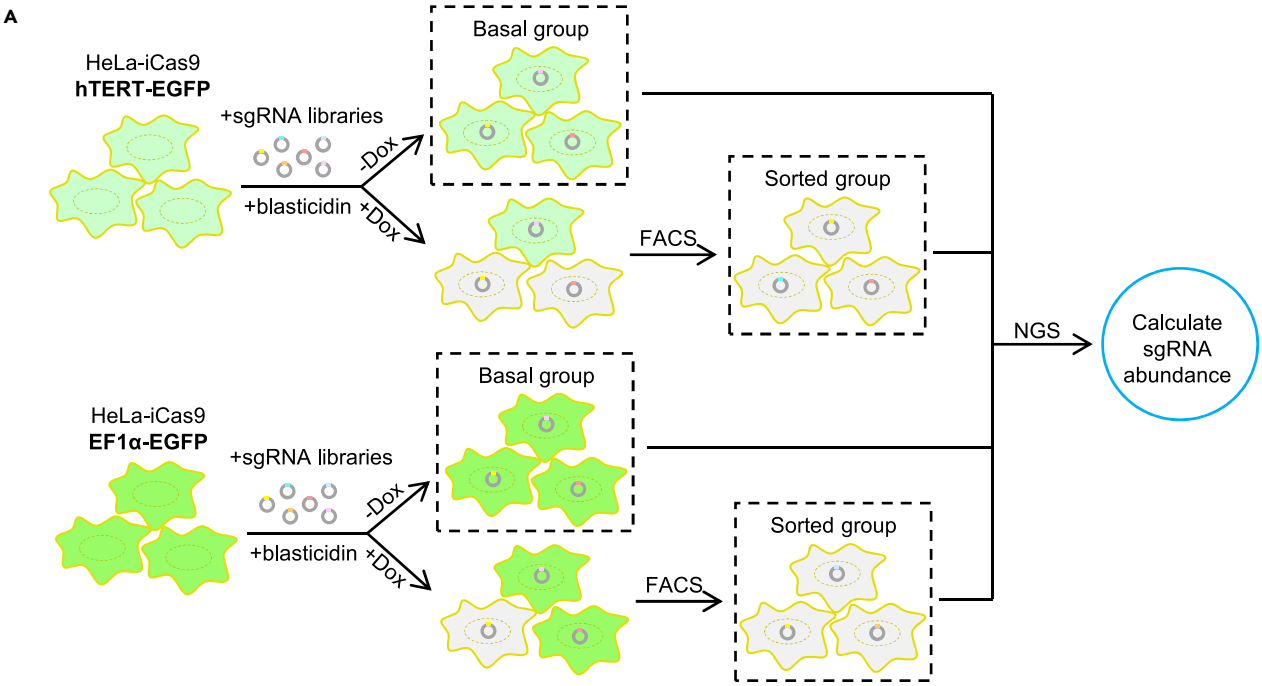
A
HeLa-iCas9
hTERT-EGFP
+sgRNA libraries
-Dox
+blasticidin
+Dox
Basal group
Sorted group
FACS
NGS
Calculate sgRNA abundance
HeLa-iCas9
EF1α-EGFP
+sgRNA libraries
-Dox
+blasticidin
+Dox
Basal group
Sorted group
FACS

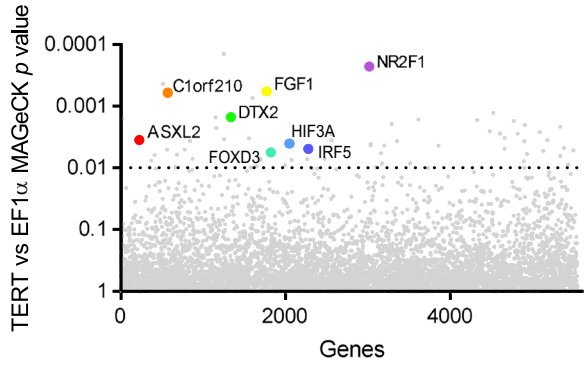
B
TERT vs EF1α MAGeCK p value
0.0001
0.001
0.01
0.1
1
0
2000
4000
Genes
NR2F1
C1orf210
FGF1
DTX2
ASXL2
HIF3A
FOXD3
IRF5

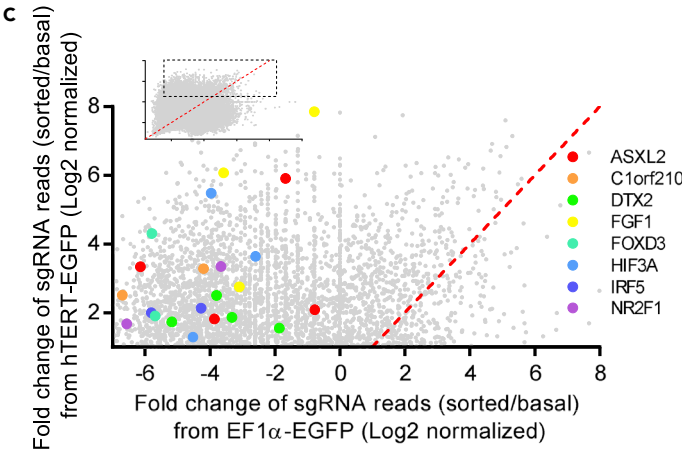
C
Fold change of sgRNA reads (sorted/basal) from hTERT-EGFP (Log2 normalized)
Fold change of sgRNA reads (sorted/basal) from EF1α-EGFP (Log2 normalized)
ASXL2
C1orf210
DTX2
FGF1
FOXD3
HIF3A
IRF5
NR2F1

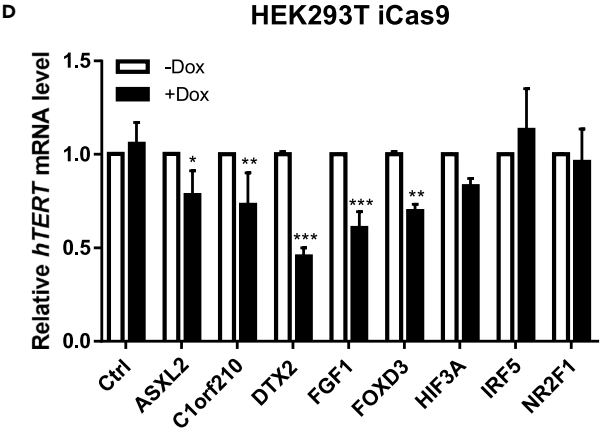
D
HEK293T iCas9
Relative hTERT mRNA level
-Dox
+Dox
Ctrl
ASXL2
C1orf210
DTX2
FGF1
FOXD3
HIF3A
IRF5
NR2F1

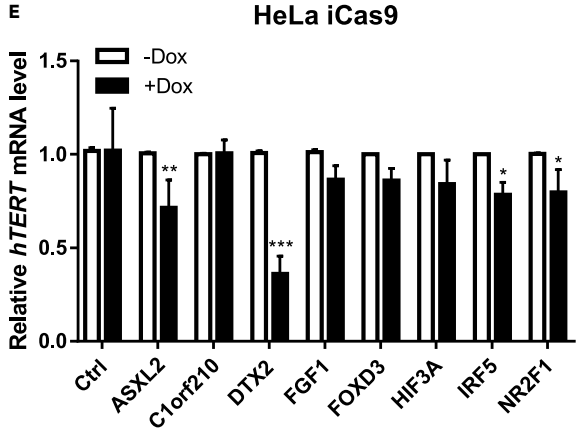
E
HeLa iCas9
Relative hTERT mRNA level
-Dox
+Dox
Ctrl
ASXL2
C1orf210
DTX2
FGF1
FOXD3
HIF3A
IRF5
NR2F1

Figure 1. An inducible CRISPR/Cas9 screen identifies positive regulators of *hTERT* transcription

(A) HeLa cells stably expressing inducible Cas9 (iCas9) and EGFP driven by the *hTERT* core promoter (hTERT-EGFP) or EF1α promoter (EF1α-EGFP) were sorted for $EGFP^+$ cells, which were then infected with lentiviral sgRNA libraries (MOI of 0.3) and selected with blasticidin. Selected cells cultured without doxycycline (Dox) served as basal groups. Dox-induced cells (1 μg/mL, 7 days) went through two rounds of FACS sorting to enrich for $EGFP^-$ cells (sorted group). All groups were subsequently analyzed by next-generation sequencing (NGS) to determine individual sgRNA abundance.

(B) MAGeCK analysis was performed (see STAR Methods) to identify top candidate genes ($p < 0.01$) in regulating *hTERT* transcription.

(C) The enrichment of specific sgRNAs for genes whose KO led to decreased *hTERT* transcription is shown in upper left corner, where each dot represents one sgRNA. Fold changes of sgRNA reads (sorted over basal groups) were transformed with Log_2 and plotted using Graphpad Prism7. The rectangular area is magnified below. The dotted red line indicates where the fold change of sgRNA reads is the same for both hTERT-EGFP and EF1α-EGFP samples.

(D and E) CRISPR KO cell pools were generated using HEK293T iCas9 (D) or HeLa iCas9 (E) cells for the genes indicated. Cells were cultured with −/+Dox (1 μg/mL) for 48 h before RT-qPCR analysis. Relative *hTERT* mRNA levels were quantified and plotted. Data were shown as mean ± SD (N = 3). p values were calculated using Student's t test. *p< 0.05; **p< 0.01; ***p< 0.001. See also Figure S1, Tables S1, and S2.

especially important for maintaining telomerase expression and in turn cell growth and viability in telomerase-positive cancer cells that harbor short telomeres.

Increase of telomerase activity is found in the majority of human cancers (Roake and Artandi, 2020). Whether modulation of DTX2 affects tumorigenicity of cancer cells remains to be addressed. Cell growth in soft agar is a gold standard *in vitro* assessment of cell malignant transformation, which is indicative for anchorage-independent growth (Anderson et al., 2007; Thierbach and Steinberg, 2009). Similar to *hTERT* knockdown, *DTX2* knockdown significantly hampered the colony forming ability of MDA-MB-231 (Figure S1Q) and HeLa (Figure S1R) cells. These data suggested that targeting DTX2 suppressed anchorage-independent growth of cancer cells.

DTX2 promotes *hTERT* transcription dependent of both RING and WWE domains

To further probe the activity of DTX2, Flag-HA (FH)-tagged DTX2 were expressed in HeLa and HT-1080 cells. Compared with the control group, DTX2 significantly upregulated *hTERT* mRNA level and telomerase activity (Figures 2E–2G and S3A–S3C). Moreover, cells with DTX2 expression also exhibited a faster rate of telomere lengthening (Figures 2H and S3D). Next, we examined two DTX2 KO clones (#20 and #39) and found markedly reduced *hTERT* mRNA level and telomerase activity, as well as accelerated telomere shortening (Figures 2I–2K and S3E). To exclude possible CRISPR/Cas9 off-target effects, FH- or SFB-tagged DTX2 were reintroduced in DTX2 KO line #20. Rescue expression of DTX2 was able to elevate *hTERT* mRNA level and telomerase activity and maintain telomere length (Figures 2L–2O and S3F–S3I). These data together support the notion that DTX2 positively regulates *hTERT* transcription in telomerase-positive cancer cells.

DTX2 has two N-terminal WWE motifs, a low complexity region (LC) and a C-terminal RING finger (Figure 3A) (Schultz et al., 2000). We compared three truncation mutants of DTX2 for their ability to rescue DTX2 KO cells. DTX2 mutants lacking regions containing the RING or WWE domains failed to rescue the decrease in *hTERT* mRNA level, telomerase activity, or telomere length in DTX2 KO cells (Figures 3B–3E). These data indicate that both RING and WWE domains are indispensable to DTX2 function.

DTX2 can localize to the nucleus and bind to the *hTERT* core promoter

DTX2 has three potential nuclear localization signals (NLS) (Lin and Hu, 2013) and is predicted to localize in the nucleoplasm based on the Human Protein Atlas (Thul and Lindskog, 2018). Because none of the commercially available DTX2 antibodies worked satisfactorily in our assays (data not shown), we examined the subcellular localization of DTX2 in HeLa cells expressing Flag-HA-tagged full-length DTX2 or truncation mutants. For comparison, the central region deletion mutant (ΔCEN) was also included (Figure 4A). Immunofluorescence (IF) assay revealed that full-length DTX2 signals were more prominent in the nucleus (Figure 4B). Cell fractionation assay showed that full-length DTX2 signals were readily detectable in both cytosolic and nuclear fractions (Figure 4C). Interestingly, respective deletion of the WWE, RING, and LC domains had little effect on DTX2 localization, whereas the ΔCEN mutant showed drastically reduced nuclear DTX2 signals in both IF and fractionation assays (Figures 4B and 4C).

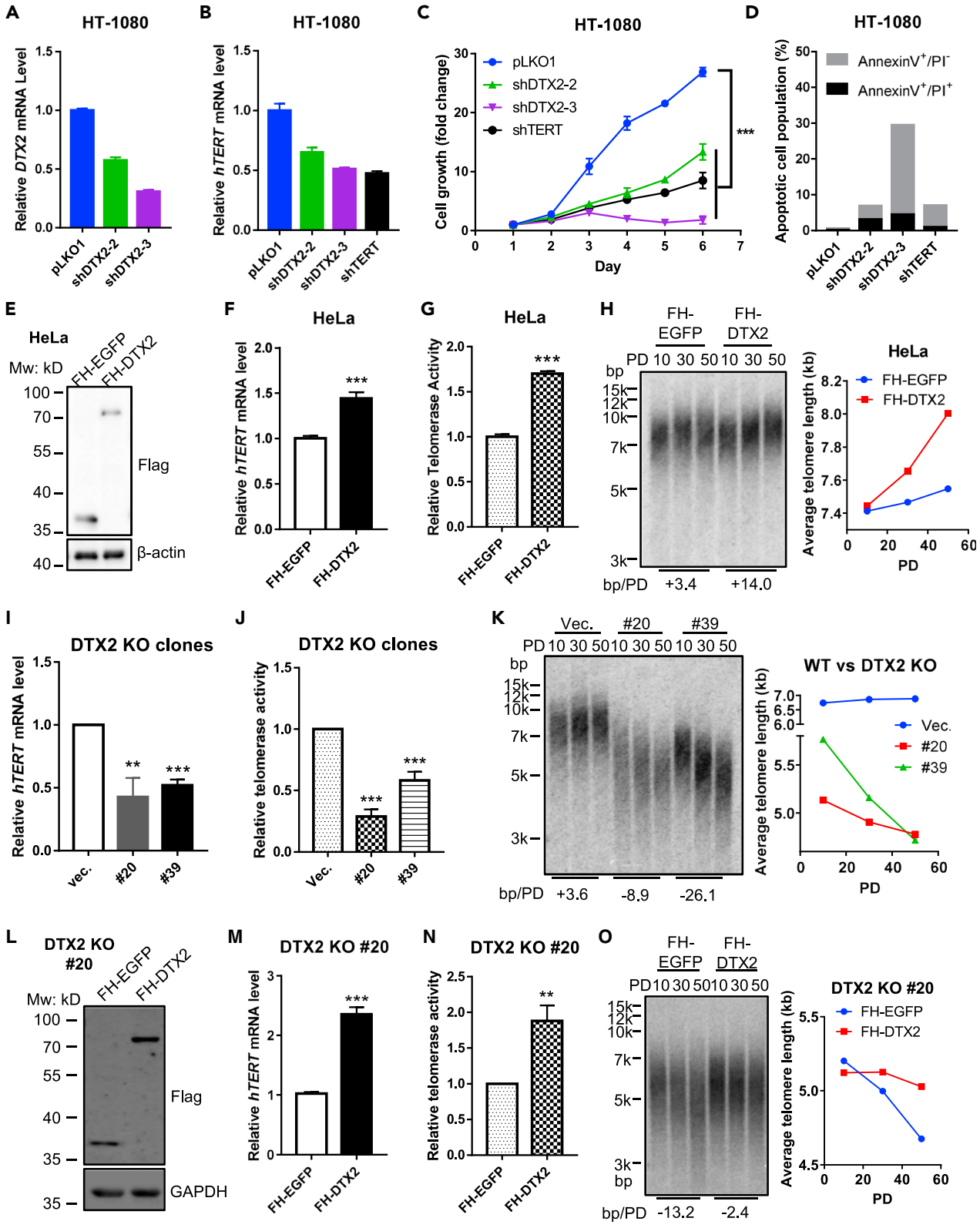
A
HT-1080
Relative DTX2 mRNA Level
pLKO1
shDTX2-2
shDTX2-3
B
HT-1080
Relative hTERT mRNA level
pLKO1
shDTX2-2
shDTX2-3
shTERT
C
HT-1080
Cell growth (fold change)
pLKO1
shDTX2-2
shDTX2-3
shTERT
***
Day
D
HT-1080
Apoptotic cell population (%)
AnnexinV+/PI-
AnnexinV+/PI+
pLKO1
shDTX2-2
shDTX2-3
shTERT
E
HeLa
Mw: kD
FH-EGFP
FH-DTX2
100
70
55
40
35
40
Flag
β-actin
F
HeLa
Relative hTERT mRNA level
***
FH-EGFP
FH-DTX2
G
HeLa
Relative Telomerase Activity
***
FH-EGFP
FH-DTX2
H
FH-EGFP
FH-DTX2
PD 10 30 50 10 30 50
bp
15k
12k
10k
7k
5k
3k
bp/PD
+3.4
+14.0
HeLa
Average telomere length (kb)
FH-EGFP
FH-DTX2
PD
I
DTX2 KO clones
Relative hTERT mRNA level
**
***
vec.
#20
#39
J
DTX2 KO clones
Relative telomerase activity
***
***
Vec.
#20
#39
K
Vec.
#20
#39
PD 10 30 50 10 30 50 10 30 50
bp
15k
12k
10k
7k
5k
3k
bp/PD
+3.6
-8.9
-26.1
WT vs DTX2 KO
Average telomere length (kb)
Vec.
#20
#39
PD
L
DTX2 KO #20
Mw: kD
FH-EGFP
FH-DTX2
100
70
55
40
35
35
Flag
GAPDH
M
DTX2 KO #20
Relative hTERT mRNA level
***
FH-EGFP
FH-DTX2
N
DTX2 KO #20
Relative telomerase activity
**
FH-EGFP
FH-DTX2
O
FH-EGFP
FH-DTX2
PD 10 30 50 10 30 50
15k
12k
10k
7k
5k
3k
bp
bp/PD
-13.2
-2.4
DTX2 KO #20
Average telomere length (kb)
FH-EGFP
FH-DTX2
PD

Figure 2. DTX2 positively regulates *hTERT* transcription and is necessary for cancer cell growth

(A–D) HT-1080 cells stably expressing *DTX2* or *hTERT* shRNAs were generated. Cells infected with pLKO1 vector viruses served as controls. Relative *DTX2* (A) and *hTERT* (B) mRNA levels were determined by RT-qPCR. Cell growth curve was examined by CCK8 assay (C). Data were shown as mean ± SD (N = 4). ***p< 0.001. The Annexin V^+/PI^- or Annexin V^+/PI^+ cells were measured by flow cytometry and defined as early or late apoptotic cells, respectively (D).

(E–H) HeLa cells expressing Flag-HA-tagged DTX2 (FH-DTX2) or EGFP (FH-EGFP) were generated. Protein expression was examined by western blotting with an anti-Flag antibody (E). Relative *hTERT* mRNA levels (F) and telomerase activity (G) were determined by RT-qPCR and qTRAP, respectively. Data were shown as mean ± SD (N = 3). ***p< 0.001. Telomere restriction fragment (TRF) analysis was performed to assess average telomere length at the indicated population doublings (PDs) with quantification using ImageQuant 5.2 (H).

(I–K) Two DTX2 knockout (KO) HeLa cell lines (#20 & #39) were generated. Empty px458 vector transfected cells served as controls. All cells were examined for relative *hTERT* mRNA level (I), telomerase activity (J), and average telomere length (K) as above. Data were shown as mean ± SD (N = 3). **p< 0.01; ***p< 0.001.(L–O) FH-EGFP or FH-DTX2 were ectopically expressed in DTX2 KO line #20. Protein expression (L), relative *hTERT* mRNA level (M), telomerase activity (N), and average telomere length (O) were assessed as above. Data are shown as mean ± SD (N = 3). **p< 001; ***p< 0.001. For all panels, p values were calculated using Student's t test, and average telomere length change is given beneath TRF blots. See also Figures S2 and S3.

Expression of the ΔCEN mutant also failed to upregulate *hTERT* mRNA level and telomerase activity in parental HeLa cells or rescue the decrease of *hTERT* mRNA level and telomerase activity in DTX2 KO cells (Figures 4D–4G), indicating the importance of nuclear targeting for DTX2 function. DTX2 might regulate telomerase expression through association with the chromatin; we therefore carried out chromatin association assays using the FH-DTX2-expressing DTX2 KO line (Figure 4H). As expected, FH-DTX2 was readily detectable in the cytosolic fraction (CE). A significant amount of DTX2 proteins could also be detected in the micrococcal nuclease-resistant insoluble chromatin fraction, suggesting likely association of DTX2 with heterochromatin regions. Because the *hTERT* locus is embedded in a region of condensed chromatin (Zhang et al., 2016), we next tested whether DTX2 could bind to the *hTERT* promoter region via ChIP-qPCR. With FH-DTX2 rescue expression, anti-HA ChIP signals were stronger than controls in the *hTERT* core promoter region (−476 to −242, −113 to +54), but similar to controls at regions farther away from *hTERT* TSS (Figure 4I), suggesting that DTX2 may directly regulate *hTERT* transcription through binding to the *hTERT* promoter.

To understand how DTX2 regulates *hTERT* transcription, we tested whether DTX2 could cause epigenetic alternations on the *hTERT* promoter. ChIP-qPCR analysis revealed that H3K4 tri-methylation level was significantly upregulated, whereas H3K9 tri-methylation level was decreased within *hTERT* core promoter region (−476 to −242, −113/+54, relative to *hTERT* TSS), suggesting the transcription activation of *hTERT* upon DTX2 expression (Figures 4J and 4K). Although H3K27 tri-methylation level did not show apparent changes in the promoter region, the binding of phosphorylated Pol II-S2 (indicative of transcription elongation) was upregulated at the 3′-end of *hTERT* gene locus (Figure 4L), suggesting that DTX2 promotes *hTERT* transcription by recruiting Pol II with productive elongating activity.

BioID-mediated proximity labeling identifies DTX2-associating partners

DTX2 lacks a DNA-binding domain; we therefore hypothesized that it might be targeted to the *hTERT* promoter through association with other DNA-binding proteins. To search for DTX2-recruiting factors, we performed BioID-mediated proximity labeling (Gingras et al., 2019; Kim et al., 2016) using HeLa DTX2 KO cells expressing BioID-DTX2 fusion proteins. DTX2 nearby proteins (<10 nm) were labeled with biotin, captured by streptavidin, and subjected to mass spectrometry analysis (Figure 5A). The proximal proteome of BioID-DTX2 exhibited great divergence from the control group (Figure S4A), with 180 proteins showing ≥3-fold higher relative abundance (Figure 5B, Table S3). Functional enrichment analysis (Pathan et al., 2015) revealed that ~10% of the DTX2-interacting partners possessed transcription factor activity, with 43 candidates implicated in transcriptional regulation (e.g., CREB regulated transcription coactivators, NF-I family, etc.) (Figure 5C). Notably, the list also contains several players involved in Notch signaling (e.g., NOTCH1-3, CTBP1, NUMB, and NCOR2), consistent with findings that *Drosophila* Deltex and human DELTEX family members interact with Notch (Matsuno et al., 1998; Zweifel et al., 2005).

DTX2 promotes *hTERT* transcription independent of Notch signaling

Drosophila Deltex activates Notch signaling by initiating endocytosis of the Notch receptor (Hori et al., 2004), whereas human DTX1 suppresses Notch/HES1 signaling to block osteosarcoma invasiveness (Zhang et al., 2010). To probe whether DTX2 could also regulate Notch signaling, we constructed a luciferase reporter driven by the promoter of the canonical Notch target *HES1* (HES1P-wt), which contains the RBP-J binding site and can be activated by the Notch intracellular domain (NICD) (Luo et al., 2017). As expected, NICD expression led to significantly higher luciferase activities in cells expressing HES1P-wt, but not

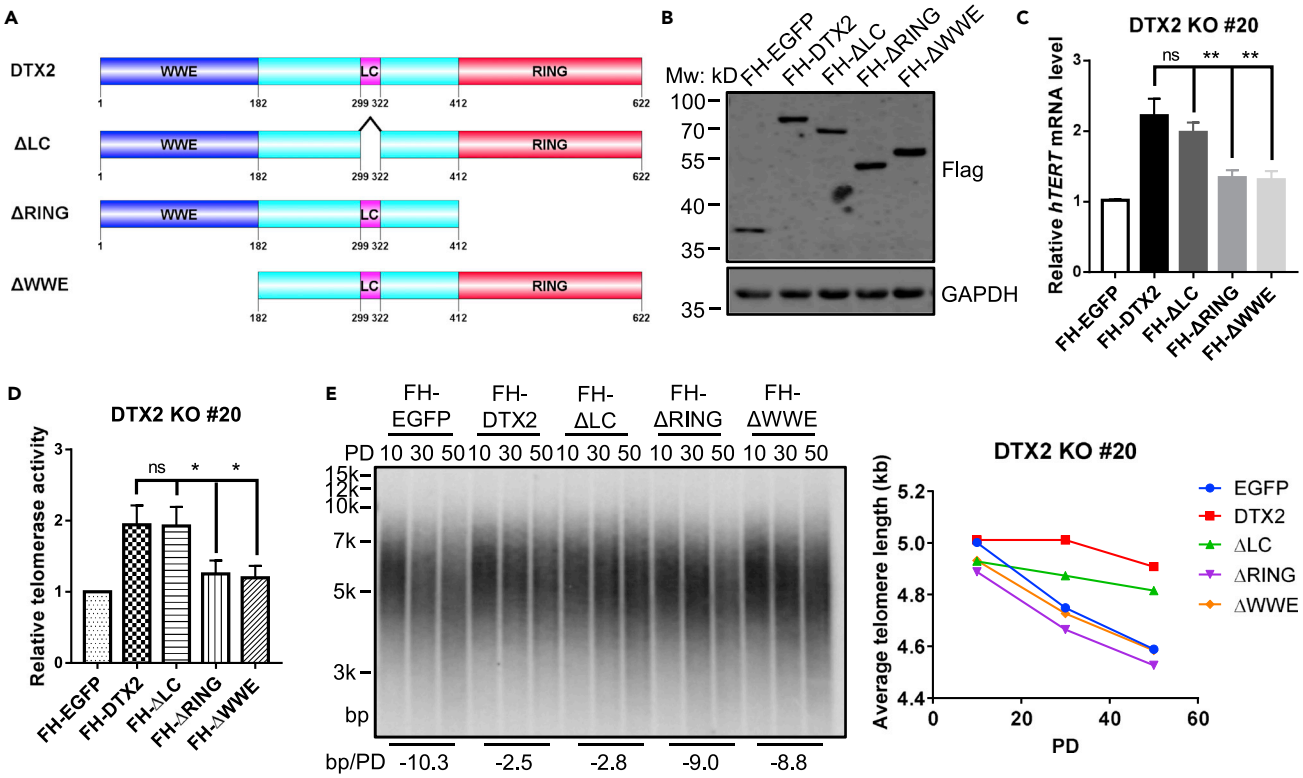

Figure 3. DTX2 promotes *hTERT* transcription dependent of both RING and WWE domains

(A) Schematic diagram of full-length and truncated DTX2 proteins. WWE, two tandem WWE motifs. LC, low complexity region. RING, region containing RING-H2 finger and C-terminal region.

(B–E) Full-length FH-DTX2 and truncation mutants were ectopically expressed in DTX2 KO line #20. Protein expression (B), relative *hTERT* mRNA level (C), telomerase activity (D), and average telomere length (E) were assessed. Data were shown as mean ± SD (N = 3). p values were calculated using Student's t test. *p< 0.05; **p< 0.01; n.s., not significant. Average telomere length change is given beneath the TRF blot.

HES1P-mut with the RBP-J binding site mutated (GTGGGAA to GTGAAAA) (Luo et al., 2017), confirming the specificity of the reporter for Notch activation (Figure S4B). Co-expressing full-length DTX2 with the HES1P-wt reporter, however, had little effect on the luciferase activity (Figures S4C and S4D). Furthermore, overexpression or depletion of DTX2 respectively augmented or suppressed *hTERT* expression but minimally impacted *HES1* mRNA levels (Figures S4E and S4F). These data argue against DTX2 functioning as a regulator of canonical Notch signaling.

Next, we examined whether Notch signaling played a role in regulating *hTERT* transcription. When HeLa cells were treated with Dibenzazepine (DBZ), the γ-secretase inhibitor that can suppress Notch receptor release (Groth et al., 2010), *HES1* mRNA level was drastically reduced, whereas *DTX2* and *hTERT* mRNA levels as well as telomerase activities remained unchanged (Figures 5D and 5E); this is supported by studies in human endothelial cells that overexpression of NOTCH had no effect on *hTERT* transcription (Giunco et al., 2015). Taken together, our data indicate that DTX2 likely regulates *hTERT* transcription independent of canonical Notch signaling.

DTX2 interacts with NFIC to regulate *hTERT* transcription

All four nuclear factor I (NF-I) family members, which have been implicated in development and cancer but never in telomerase regulation (Chen et al., 2017), were identified as DTX2-associating proteins (Table S3). NFIA, NFIB, and NFIC were among the top candidates and could each co-IP with DTX2 (Figure S4G). However, only NFIC overexpression significantly upregulated *hTERT* mRNA level and telomerase activity in HeLa cells, and rescued the decrease in *hTERT* mRNA level and telomerase activity in DTX2 KO cells (Figures 5F–5I), pointing to NFIC as the likeliest family member to facilitate DTX2-mediated telomerase regulation.

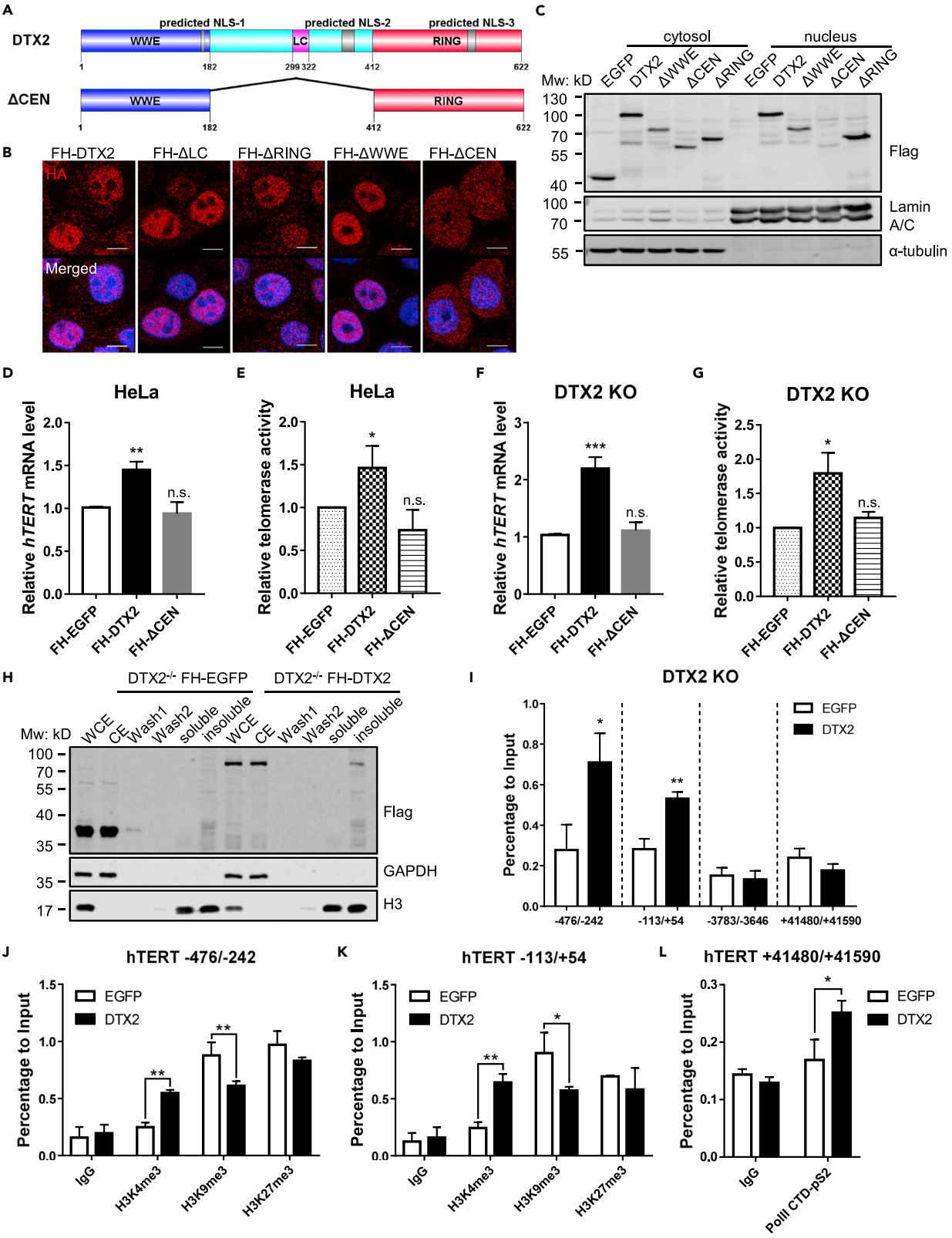
A
DTX2
predicted NLS-1
predicted NLS-2
predicted NLS-3
WWE
LC
RING
1
182
299 322
412
622
ΔCEN
WWE
RING
1
182
412
622
B
FH-DTX2
FH-ΔLC
FH-ΔRING
FH-ΔWWE
FH-ΔCEN
HA
Merged
C
cytosol
nucleus
Mw: kD
EGFP
DTX2
ΔWWE
ΔCEN
ΔRING
130
100
70
55
40
Flag
Lamin A/C
α-tubulin
D
HeLa
Relative hTERT mRNA level
FH-EGFP
FH-DTX2
FH-ΔCEN
n.s.
E
HeLa
Relative telomerase activity
F
DTX2 KO
Relative hTERT mRNA level
G
DTX2 KO
Relative telomerase activity
H
DTX2-/- FH-EGFP
DTX2-/- FH-DTX2
WCE
CE
Wash1
Wash2
soluble
insoluble
Flag
GAPDH
H3
I
DTX2 KO
Percentage to Input
EGFP
DTX2
-476/-242
-113/+54
-3783/-3646
+41480/+41590
J
hTERT -476/-242
IgG
H3K4me3
H3K9me3
H3K27me3
K
hTERT -113/+54
L
hTERT +41480/+41590
PolII CTD-pS2

Figure 4. DTX2 can localize to the nucleus and bind to the *hTERT* core promoter

(A) Schematic diagram of predicted nuclear localization signals (NLS) of DTX2 and the ΔCEN mutant.

(B and C) Full-length FH-DTX2 and its truncation mutants were expressed in HeLa cells. The localization of various DTX2 proteins was examined by immunostaining with an anti-HA antibody (scale bar: 10 μm) (B) and western blotting following cell fractionation using the indicated antibodies (C). FH-EGFP-expressing cells served as negative controls for fractionation.

(D and E) HeLa cells expressing full-length DTX2 or the ΔCEN mutant were assayed by RT-qPCR and qTRAP to determine the relative *hTERT* mRNA level (D) and telomerase activity (E). Data were shown as mean ± SD (N = 3). p values were calculated using Student's t test. *p< 0.05; **p<0.01; n.s., not significant.

(F and G) DTX2 KO cells (#20) expressing full-length DTX2 or the ΔCEN mutant were assayed by RT-qPCR and qTRAP to determine the relative *hTERT* mRNA level (F) and telomerase activity (G). Data were shown as mean ± SD (N = 3). p values were calculated using Student's t test. *p< 0.05; ***p< 0.001; n.s., not significant.

(H) DTX2 KO line #20 expressing FH-EGFP or FH-DTX2 were fractionated for the chromatin association assay. Various fractions were subjected to immunoblot analysis with the indicated antibodies. WCE, whole cell extract. CE, cytosolic extract. Wash 1 & 2, nucleoplasmic fraction. Soluble & insoluble, chromatin fractions sensitive or resistant to micrococcal nuclease digestion.

(I) ChIP-qPCR analysis was done using cells from (H) and an anti-HA antibody. Primers span areas within the *hTERT* core promoter region (−113/+54 and −476/−242), upstream (~3.7 kb) of *hTERT* TSS (−3,783/−3,646), or in the last exon (+41,480/+41,590). Enrichment of specific regions was normalized to input. Data were shown as mean ± SD (N = 3). p values were calculated using Student's t test. *p< 0.05; **p< 0.01.

(J and K) ChIP-qPCR analysis was done using cells from (H) and anti-H3K4me3, anti-H3K9me3, and anti-H3K27me3 antibodies. Primers span areas within the *hTERT* core promoter region [−113/+54 (J) and −476/−242 (K)]. Enrichment of specific regions was normalized to input. Data were shown as mean ± SD (N = 2). p values were calculated using Student's t test. *p< 0.05; **p< 0.01. (L) ChIP-qPCR analysis was done using cells from (H) and anti-Pol II-pS2 antibody. Primers span areas in the last exon of *hTERT* (+41,480/+41,590). Enrichment of specific regions was normalized to input. Data were shown as mean ± SD (N = 2). p values were calculated using Student's t test. *p< 0.05.

NF-I proteins contain highly conserved DNA-binding and dimerization regions in the N-terminus that include the pre-N and MH1 domains, but their C-terminal CTF transcription modulation regions vary considerably (Chen et al., 2017; Marchler-Bauer et al., 2017). To test which domain is required for DTX2-NFIC interaction, we constructed FH-tagged NFIC truncation mutants with the pre-N (Δpre-N), MH1 (ΔMH1), or CTF (ΔCTF) region deleted (Figure S5A). Co-IP experiment showed that pre-N or MH1 domain deletion severely impaired interaction between NFIC and DTX2, indicating that both regions were required for efficient DTX2-NFIC interaction (Figure S5B). In reciprocal co-IP experiments using cells co-expressing full-length NFIC with full-length or truncated DTX2, DTX2-NFIC interaction was completely abolished in the absence of the DTX2 central region, but not RING or WWE domains (Figure S5C). In fact, the central region alone was sufficient to co-IP with NFIC (Figure S5D). Given the importance of the CEN domain to DTX2 nuclear targeting and function, these observations suggest that DTX2 nuclear targeting enabled its interaction with NFIC.

DTX2 increases NFIC association with the *hTERT* promoter to augment *hTERT* transcription

To further confirm the role of NFIC in DTX2-mediated telomerase regulation, we generated DTX2/NFIC double KO (DKO) HeLa cells (Figures S6A and S6B). Unlike in DTX2 KO cells, expressing DTX2 in DKO cells did not rescue *hTERT* mRNA level or telomerase activity (Figures 6A, 6B, and S6C). In contrast, expression of NFIC significantly upregulated the level of both *hTERT* mRNA and telomerase activity in DKO cells, indicating that NFIC likely functioned downstream of DTX2. When we examined DKO cells by ChIP-qPCR, we could no longer detect any enrichment of DTX2 signals at the *hTERT* core promoter region (Figure 6C), suggesting that NFIC was crucial to DTX2 association with the *hTERT* promoter.

NFI family members share identical DNA-binding motifs containing the same palindromic sequence and can bind DNA with half sites (albeit at lower affinity) (Gronostajski, 2000; Zenker et al., 2019). SELEX and ChIP-seq data from the JASPAR database (Fornes et al., 2020) indicate four potential DNA-binding motifs for NFIC, with T/CTGGC being the half-site consensus sequence (Figure S6D). Notably, three CTGGC motifs are located within the *hTERT* core promoter region (−389, −295, and −19 relative to ATG), which overlap with DTX2-associating regions (−476 to −242, −113 to +54) (Figure 4I). When we probed NFIC binding to the *hTERT* promoter by ChIP-qPCR using HeLa cells expressing FH-NFIC, we found enriched NFIC signals in the same regions bound by DTX2 (Figure 6D). Moreover, FH-NFIC bound to DNA probes containing CTGGC motifs *in vitro* (Figure 6E). Of the three potential binding sites, DNA probes with flanking sequences of both −19 and −389 (relative to ATG) could be bound by FH-NFIC but not FH-EGFP. More importantly, anti-HA antibodies together with DNA-bound FH-NFIC formed super-shift complexes, indicating specific and direct interaction between NFIC and the DNA probes.

To determine how DTX2 functions through NFIC, we reintroduced tetracycline-induced DTX2-SFB (iDTX2-SFB) into DTX2 KO cells and measured intensity of NFIC binding to the *hTERT* promoter by ChIP-qPCR.

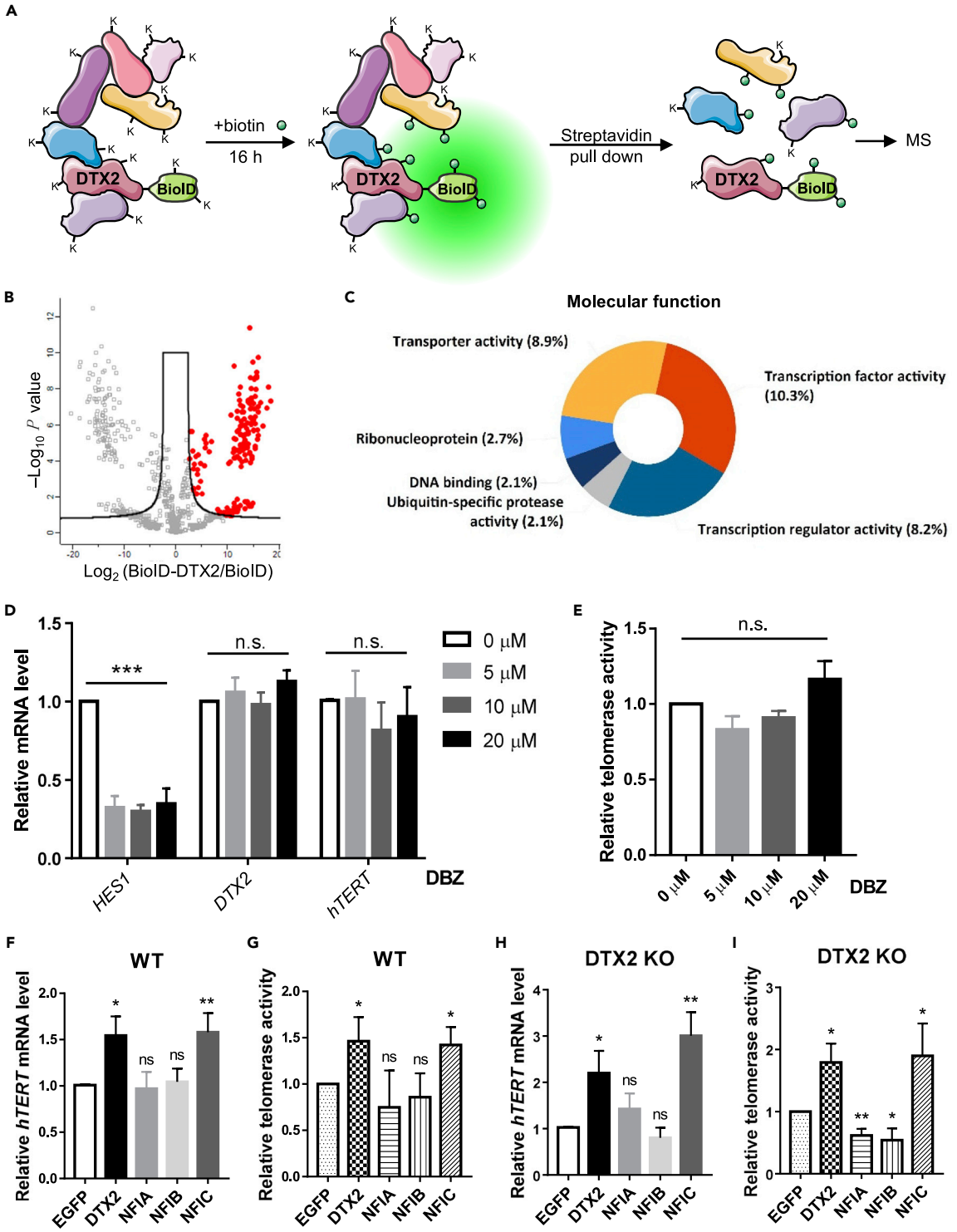

Figure 5. BioID-mediated proximity-labeling identifies DTX2-associating partners

(A) BioID was fused to the N-terminus of full-length DTX2 and expressed in HeLa cells. In the presence of biotin, BioID labels nearby proteins on lysine (K) residues. Biotinylated proteins are then pulled down by streptavidin-coupled beads and analyzed by mass spectrometry (MS). Each group was done in triplicates.

(B) Proteins identified in the BioID-DTX2 group were compared with those for BioID alone in a volcano plot graphed using Perseus. Red dots indicate highly enriched proteins (FOT>3, refer to STAR Methods).

Figure 5. *Continued*

(C) Molecular function analysis was performed using the FUNRICH software to analyze the proteins enriched in the BioID-DTX2 group from (B).

(D and E) HeLa cells treated for 24 h with different concentrations of the Notch inhibitor DBZ were harvested to assess the relative mRNA levels of *HES1*, *DTX2*, and *hTERT* (D) and telomerase activities (E). Data were shown as mean ± SD (N = 3). p values were calculated using two-way ANOVA. ***p< 0.001; n.s., not significant.

(F and G) HeLa cells overexpressing DTX2 or NF-I family proteins were assessed for relative *hTERT* mRNA levels (F) and telomerase activities (G). Data were shown as mean ± SD (N = 3).

(H and I) DTX2 KO cells overexpressing DTX2 or NF-I family proteins were assessed for relative *hTERT* mRNA levels (H) and telomerase activities (I). Data were shown as mean ± SD (N = 3). For panels (F–I), p values were calculated using Student's t test. *p< 0.05; **p< 0.01; n.s., not significant. See also Figures S4, S5, and Table S3.

Upon Dox addition, NFIC-ChIP signals were significantly increased on the *hTERT* promoter (Figures 6F and 6G). Although NFIC expression alone upregulated *hTERT* expression in DTX2 KO cells, rescued DTX2 expression further elevated *hTERT* mRNA level (Figure 6H), suggesting that DTX2 might augment *hTERT* transcription by facilitating NFIC binding to the *hTERT* promoter.

To further examine whether the binding of DTX2-NFIC complex on *hTERT* promoter could lead to epigenetic changes, we performed ChIP-qPCR analysis in DTX2/NFIC DKO cells with re-expression of DTX2 (Figure 6I). As mentioned earlier, re-expression of DTX2 in DKO cells could not rescue *hTERT* transcription, whereas re-expression of NFIC could rescue this phenotype (Figure 6A). Consistently, we observed significant increase of H3K4me3 and decrease of H3K9me3 within the *hTERT* promoter region (Figure 6J), as well as accumulation of phosphorylated Pol II-S2 at the 3′-end of *hTERT* gene in the NFIC re-expression group (Figure 6K). Taken together, these data supported that DTX2-NFIC axis corporately regulates epigenetic changes in promoting *hTERT* transcription.

DTX2 mediates K63-linked ubiquitination of NFIC to enhance *hTERT* transcription

Although mammalian DTX family proteins can function as E3 ligases (Cui et al., 2012; Luo et al., 2017; Takeyama et al., 2003), very little is known about their physiological targets. To determine whether DTX2 could regulate NFIC through ubiquitination, we first carried out ubiquitination assays using HEK293T cells co-expressing HA-tagged ubiquitin (HA-Ub) with GST-NFIC and DTX2-SFB. Increased ubiquitin signals could be detected on GST-NFIC upon DTX2 expression (Figure 7A, left), indicating DTX2-dependent ubiquitination of NFIC in these cells. Two of the most common linkage types, K48- and K63-linked ubiquitination, are often associated with proteasome degradation and nonproteolytic functions, respectively (Wang et al., 2012). To understand the linkage types of DTX2-dependent ubiquitination, HA-tagged ubiquitin mutants containing only K48 or K63 were examined. With HA-Ub-K48, NFIC ubiquitination level appeared comparable between DTX2- and EGFP-expressing cells (Figure 7A, middle), suggesting involvement of other linkages not affecting NFIC stability. This is consistent with findings in iDTX2-SFB cells (Figure 6F), where FH-NFIC protein level remained unchanged upon dox-induced DTX2 expression. When HA-Ub-K63 was co-transfected with NFIC and DTX2, markedly increased NFIC ubiquitination was detected (Figure 7A, right), pointing to K63 as the primary linkage type.

Previous studies have identified key residues within the mouse Dtx2/Deltex2 RING domain (I411/M454), whose mutations blocked Dtx2 E3 ligase activity (Luo et al., 2017). When the orthologous residues were mutated in the RING domain (I/M*, I414R/M457R) of DTX2, NFIC ubiquitination was noticeably reduced with either HA-Ub or HA-Ub-K63 (Figure 7B), indicating that the E3 ligase activity of DTX2 was essential for K63-linked ubiquitination of NFIC. In addition, re-expression of DTX2 I/M* could not rescue *hTERT* transcription in DTX2 KO cells (Figure S7A), suggesting the E3 ligase activity is required for *hTERT* transcription regulation. To map the NFIC domain required for ubiquitination, we co-transfected DTX2-SFB and HA-Ub into HEK293T cells with GST-tagged NFIC and its truncation mutants. Although ubiquitination of the ΔpreN and ΔCTF mutants remained efficient, ubiquitination of the ΔMH1 mutant was markedly impaired (Figure S7B), suggesting that the MH1 domain was critical to DTX2-mediated NFIC ubiquitination.

Based on *in silico* search using PhosphoSitePlus (Hornbeck et al., 2015) and UbiSite (Akimov et al., 2018), K to R point mutants of the five putative ubiquitin-conjugation sites on NFIC were generated. Consistently, two mutants within the MH1 domain, K65R and K99R, showed drastically reduced NFIC ubiquitination (Figure 7C), indicating these two residues as primary DTX2 ubiquitination sites. We then asked whether ubiquitination of K65/K99 was important for NFIC function by expressing single and double K-R mutants in the DKO cells (Figure 7D). Unlike wild-type (WT) NFIC, all three mutants failed to enhance *hTERT* mRNA level or telomerase activity and

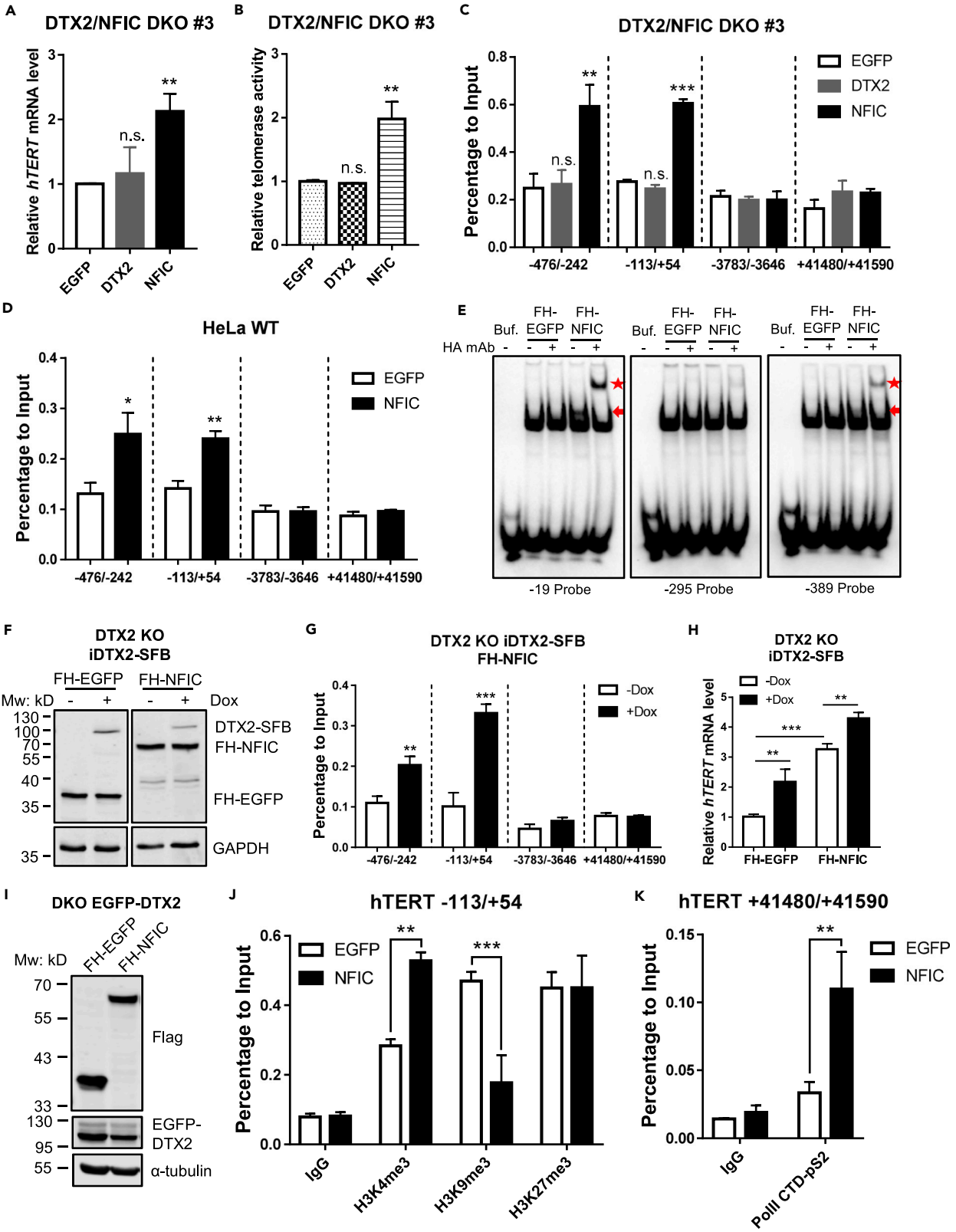
A
DTX2/NFIC DKO #3
Relative hTERT mRNA level
n.s.
**
EGFP
DTX2
NFIC
B
DTX2/NFIC DKO #3
Relative telomerase activity
n.s.
**
EGFP
DTX2
NFIC
C
DTX2/NFIC DKO #3
Percentage to Input
n.s.
**
n.s.
***
EGFP
DTX2
NFIC
-476/-242
-113/+54
-3783/-3646
+41480/+41590
D
HeLa WT
Percentage to Input
*
**
EGFP
NFIC
-476/-242
-113/+54
-3783/-3646
+41480/+41590
E
Buf.
FH-EGFP
FH-NFIC
HA mAb
-19 Probe
-295 Probe
-389 Probe
F
DTX2 KO
iDTX2-SFB
FH-EGFP
FH-NFIC
Mw: kD
Dox
130
100
70
55
40
35
35
DTX2-SFB
FH-NFIC
FH-EGFP
GAPDH
G
DTX2 KO iDTX2-SFB
FH-NFIC
Percentage to Input
**
***
-Dox
+Dox
-476/-242
-113/+54
-3783/-3646
+41480/+41590
H
DTX2 KO
iDTX2-SFB
Relative hTERT mRNA level
-Dox
+Dox
**
***
**
FH-EGFP
FH-NFIC
I
DKO EGFP-DTX2
Mw: kD
FH-EGFP
FH-NFIC
70
55
43
33
130
95
55
Flag
EGFP-
DTX2
α-tubulin
J
hTERT -113/+54
Percentage to Input
**
***
EGFP
NFIC
IgG
H3K4me3
H3K9me3
H3K27me3
K
hTERT +41480/+41590
Percentage to Input
**
EGFP
NFIC
IgG
PolII CTD-pS2

Figure 6. DTX2 promotes NFIC association with the *hTERT* promoter for *hTERT* transcriptional activation

(A and B) FH-tagged EGFP, DTX2, or NFIC was ectopically expressed in the DTX2/NFIC double knockout (DKO) line #3. Relative *hTERT* mRNA level (A) and telomerase activity (B) were assessed. Data were shown as mean ± SD (N = 3). **p< 0.01; n.s., not significant.

(C) Cells from (A) were also examined by ChIP-qPCR with an anti-HA antibody and primers for the indicated region (relative to *hTERT* TSS). Enrichment of the examined regions in ChIP samples was normalized to input. Data were shown as mean ± SD (N = 3). **p< 0.01; ***p< 0.001; n.s., not significant.

(D) HeLa cells stably expressing FH-NFIC were analyzed in ChIP-qPCR with an anti-HA antibody and primers for the indicated region (relative to *hTERT* TSS). Results were normalized to input. Data were shown as mean ± SD (N = 3). *p< 0.05; **p< 0.01.

(E) In the electrophoretic mobility shift assay (EMSA), cell lysate from HEK293T cells transiently expressing FH-EGFP or FH-NFIC was incubated with biotin-labeled double-stranded DNA probes containing the flanking sequences surrounding regions −19, −295, or −389 upstream of *hTERT* TSS. An anti-HA antibody was used to super-shift the protein-DNA complex. Reaction mixtures were resolved on a nondenaturing PAGE gel and blotted with streptavidin. Red arrow indicates protein-DNA complex. Red star indicates super-shifted complexes.

(F–H) Dox-inducible DTX2-SFB (iDTX2-SFB) were reintroduced into DTX2 KO cells with FH-EGFP or FH-NFIC expression. Cells were cultured with −/+Dox (1 μg/mL) for 48 h before western blot (F), ChIP-qPCR analysis of indicated regions (relative to *hTERT* TSS) (G), and RT-qPCR for relative *hTERT* mRNA level (H). Data were shown as mean ± SD (N = 3). **p< 0.01; ***p< 0.001. For all panels, p values were calculated using Student's t test.

(I) DTX2/NFIC DKO cells stably expressing FH-tagged EGFP or NFIC were reintroduced with EGFP-DTX2 and examined by western blot using the indicated antibodies.

(J) ChIP-qPCR analysis was done using cells from (I) and anti-H3K4me3, anti-H3K9me3, and anti-H3K27me3 antibodies. Primers span areas within the *hTERT* core promoter region (−113/+54). Enrichment of specific regions was normalized to input. Data were shown as mean ± SD (N = 2). p values were calculated using Student's t test. **p< 0.01; ***p< 0.001.

(K) ChIP-qPCR analysis was done using cells from (I) and anti-Pol II-pS2 antibody. Primers span areas in the last exon of *hTERT* (+41,480/+41,590). Enrichment of specific regions was normalized to input. Data were shown as mean ± SD (N = 2). p values were calculated using Student's t test. **p< 0.01. See also Figure S6.

were unable to bind the *hTERT* promoter (Figures 7E–7G), underlining the importance of K63-linked ubiquitination of NFIC K65/K99 and the DTX2-NFIC axis to *hTERT* transcriptional regulation.

To examine whether DTX2-NFIC axis contributes to tumorigenesis, we performed the soft agar assays using DTX2/NFIC DKO cells with re-expression of DTX2, WT or mutant NFIC to determine their contribution to tumorigenesis. As shown in Figure S7C, HeLa cells with depletion of both DTX2 and NFIC barely formed colonies in soft agar. Although re-expression of DTX2 did not promote colony formation, re-expression of NFIC was sufficient to increase colony number in DKO cells. This is consistent with our previous data that NFIC functioned downstream of DTX2 to enhance *hTERT* transcription. Compared with WT NFIC, re-expression of K65R/K99R mutant led to fewer colonies, suggesting the DTX2-mediated ubiquitination of NFIC promotes tumorigenesis.

Taken together, our data support the model: in telomerase positive cancer cells with low DTX2 expression, NFIC binds to the *hTERT* promoter (consensus half sites) with reduced affinity. Thus, *hTERT* gene is embedded in the transcription repressive chromatin with high level of H3K9 tri-methylation. Heightened DTX2 expression increases DTX2-NFIC association and K63-linked ubiquitination of NFIC K65/K99, which promotes DTX2-NFIC binding to the *hTERT* promoter. The enrichment of DTX2-NFIC complex on *hTERT* promoter increases H3K4me3 and recruits Pol II with productive elongating activity, therefore enhancing *hTERT* transcription (Figure 7H).

DISCUSSION

In this study, we carried out systematic and functional mapping of the *hTERT* transcriptional regulatory network through an inducible CRISPR/Cas9 KO screen. The inducible strategy increased the chance of identifying positive regulators whose inhibition may affect cell growth and established baseline cells to account for random drifts. The control EF1α promoter was chosen for its human origin, robust activity across different cell types, and resistance to chromatin changes (Norrman et al., 2010). The EF1α reporter cells helped exclude factors important for transcription and protein stability in general. In this screen, many uncharacterized regulators for *hTERT* transcription were identified, providing a comprehensive view of *hTERT* regulation network.

DTX2 was discovered as an important *hTERT* transcription regulator through mediating ubiquitination of transcription factor NFIC. The function of DTX2 was rarely known until a recent study revealed multiple DNA-damage-repair-related proteins as DTX2-interacting partners and ubiquitination substrates (Ahmed et al., 2020). Especially, one of the substrates is poly-ADP ribose polymerase 1 (PARP1), which participates in DSB repair at telomeres (Doksani and de Lange, 2016; Harvey et al., 2018). Therefore, DTX2 may help maintain telomere homeostasis through NFIC-mediated *hTERT* transcriptional activation and PARP1-dependent telomere maintenance.

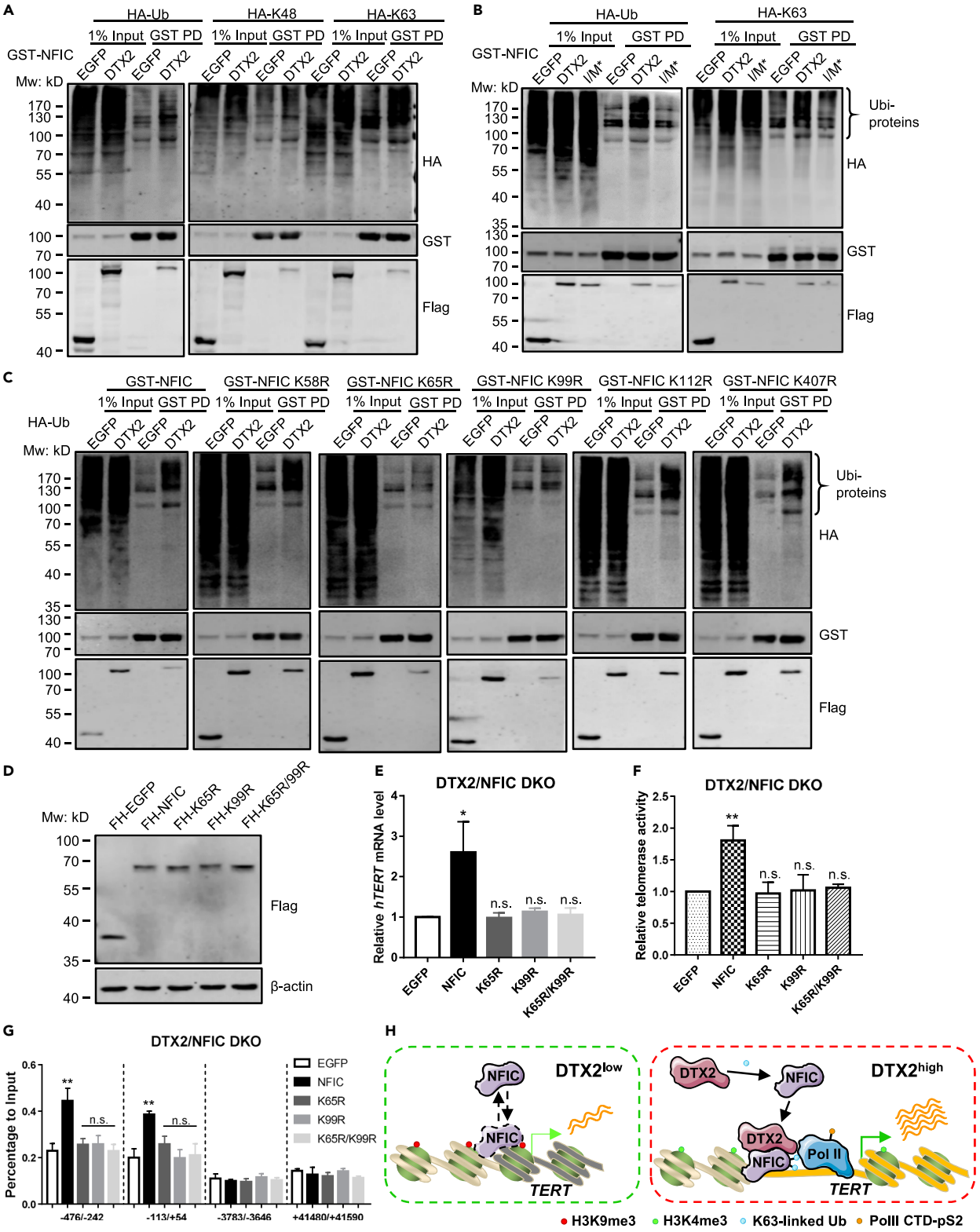

Figure 7. DTX2 mediates K63-linked ubiquitination of NFIC to enhance *hTERT* transcription

(A) GST-NFIC was transiently co-expressed in HEK293T cells with DTX2-SFB and HA-tagged Ub or Ub K48/K63 mutants as indicated. EGFP-SFB was used as a control. Cells were harvested for GST pull-down (PD) and western blotting as shown.

Figure 7. *Continued*

(B) GST-NFIC was transiently co-expressed in HEK293T cells with SFB-tagged DTX2 or the I/M* mutant as well as HA-tagged Ub or Ub K63 mutant as indicated. I/M*, DTX2 with I414R and I457R mutations. EGFP-SFB was used as a control. Cells were harvested for GST pull-down (PD) and western blotting as shown.

(C) HA-Ub was transiently co-expressed in HEK293T cells with DTX2-SFB and GST-tagged WT or K/R point mutants of NFIC. EGFP-SFB was used as a control. Cells were harvested for GST pull-down (PD) and western blotting as shown.

(D–F) DTX2/NFIC DKO cells ectopically expressing FH-tagged WT or K/R point mutants of NFIC were examined for protein expression with an anti-Flag antibody (D), relative *hTERT* mRNA level by qPCR (E), and telomerase activity by qTRAP (F). Data were shown as mean ± SD (N = 3). *p< 0.05; **p< 0.01; n.s., not significant.

(G) ChIP-qPCR analysis was performed with an anti-HA antibody and primers for the indicated DNA regions (relative to *hTERT* TSS) using cells from (D). Data were shown as mean ± SD (N = 3). **p< 0.01; n.s., not significant. For panels E–G, p values were calculated using Student's t test.

(H) In telomerase-positive cancer cells with low DTX2 expression, NFIC binds to the consensus half sites on the *hTERT* promoter with low affinity. Increased DTX2 expression promotes its interaction with NFIC and K63-linked ubiquitination at K65 and K99 sites, which helps stabilize the binding of the DTX2-NFIC complex to the *hTERT* core promoter and enhance *hTERT* transcription. (H) In telomerase-positive cancer cells with low DTX2 expression, NFIC binds to the consensus half sites on the *hTERT* promoter with low affinity. The *hTERT* gene remains transcription repressive with hypermethylation on H3K9. Increased DTX2 expression promotes its interaction with NFIC and K63-linked ubiquitination at K65 and K99 sites, which helps stabilize the binding of the DTX2-NFIC complex to the *hTERT* core promoter. The enrichment of DTX2-NFIC further upregulates H3K4me3 level and helps recruit phosphorylated Pol II-S2, therefore enhancing *hTERT* transcription. See also Figure S7.

Our findings of NFIC as an *hTERT* transcriptional regulator downstream of DTX2 further underline the non-redundancy of NF-I proteins, which have shown opposite activities in different model systems (Chen et al., 2017). Promoter context, tissue/cell types, and interacting partners help determine their activity potential and mode of action (Chen et al., 2017). For example, NF-I members vary in their specificities for the CoRE response element of the WAP gene, depending on the presence of other transcription factors (Mukhopadhyay et al., 2001). In our case, reintroducing DTX2 in DTX2 KO cells significantly enhanced NFIC binding to the *hTERT* promoter and further increased *hTERT* transcription, due to DTX2-mediated K63-linked ubiquitination of NFIC K65/K99. Our findings support the notion that K63-linked ubiquitination may be essential to NFIC transactivation of *hTERT* expression and integral to DTX2-mediated transcriptional regulation.

Both Deltex and NFI family proteins have been implicated in cancer (Chen et al., 2017). For instance, DTX2 belongs to an 18-gene panel of prognostic biomarkers whose expression is associated with poor outcomes in metastatic breast cancer (Cheng et al., 2017). Our data also indicate that DTX2 is required for anchorage-independent growth of various cancer cells (Figures. S2Q and S2R). Tumor cells often reactivate telomerase to maintain telomere length and achieve unlimited cell proliferation. Therefore, targeting telomerase represents an attractive strategy (Guterres and Villanueva, 2020). The DTX2-NFIC axis offers a new avenue of research for telomerase inhibition through blocking DTX2-NFIC interaction. Further studies should not only shed more light on the mechanisms that govern *hTERT* expression in normal versus cancer cells but also uncover alternative therapeutics for treating cancer.

Limitations of the study

Increased expression of DTX2 is shown in various cancer types. In this study, we observed that depletion of DTX2 suppressed cancer cell growth via downregulating *hTERT* transcription especially in telomerase-positive cancer with short telomeres. We revealed the mechanism how DTX2-NFIC axis regulates *hTERT* transcription, but we did not identify the upstream signaling. Further study is needed to understand how DTX2-NFIC axis is regulated during cancer progression.

STAR★METHODS

Detailed methods are provided in the online version of this paper and include the following:

- KEY RESOURCE TABLE
- RESOURCE AVAILABILITY
  - Lead contact
  - Materials availability
  - Data and code availability
- EXPERIMENTAL MODEL AND SUBJECT DETAILS
  - Cell lines and cell culture
- METHOD DETAILS
  - CRISPR/Cas9-mediated inducible knockout screen
  - High-throughput sequencing and data analysis

SUPPLEMENTAL INFORMATION

Supplemental information can be found online at https://doi.org/10.1016/j.isci.2022.103813

ACKNOWLEDGMENTS

This work was supported by the National Key Research and Development Program of China (2018YFA0107003 to W.M.), National Natural Science Foundation of China (NSFC 31930058 to Z.S., 32170757 to W.M., 31871479 to W.M., 81871111 to F.L., 32071433 to F.L., 32070778 to S.W.), and Guangdong Basic and Applied Basic Research Foundation (2020B1515020044 to F.L., 2019A1515011552 to S.W.). The authors thank Dr. Dan Liu for her great efforts on manuscript revision, Mengjie Deng, Yingxia Wu, and Chuying Zhang for their excellent technical support, and members of the Songyang laboratory for their insightful discussions.

AUTHOR CONTRIBUTIONS

Z.S., W.M., and S.W. conceptualized the ideas, supervised the project, and edited the manuscript. F.L. and H.H. reviewed and edited the manuscript. Z.Z. designed and performed most of the experiments and wrote the manuscript. Y.L. designed and performed the CRISPR screen, and X.X. conducted the high-throughput sequencing data analysis. H.X. excluded the Notch signaling pathway in DTX2-mediated *hTERT* transcription regulation. S.W. helped with the BioID data analysis. Z.H. helped with the FACS and TRF experiment. S.L. helped with the ChIP-qPCR experiment. R.L. helped with the EMSA experiment. S.J. and J.C kindly provided ubiquitin expression plasmids and shared with the experiment procedure of ubiquitination assay. All authors discussed the results.

DECLARATION OF INTERESTS

The authors declare no competing interests.

Received: August 16, 2021
Revised: December 7, 2021
Accepted: January 20, 2022
Published: February 18, 2022

REFERENCES

Ahmed, S.F., Buetow, L., Gabrielsen, M., Lilla, S., Chatrin, C., Sibbet, G.J., Zanivan, S., and Huang, D.T. (2020). DELTEX2 C-terminal domain recognizes and recruits ADP-ribosylated proteins for ubiquitination. Sci Adv. *6*. https://doi.org/10.1126/sciadv.abc0629.

Akimov, V., Barrio-Hernandez, I., Hansen, S.V.F., Hallenborg, P., Pedersen, A.K., Bekker-Jensen, D.B., Puglia, M., Christensen, S.D.K., Vanselow, J.T., Nielsen, M.M., et al. (2018). UbiSite approach for comprehensive mapping of lysine and N-terminal ubiquitination sites. Nat. Struct. Mol. Biol. *25*, 631–640. https://doi.org/10.1038/s41594-018-0084-y.

Anderson, S.N., Towne, D.L., Burns, D.J., and Warrior, U. (2007). A high-throughput soft agar assay for identification of anticancer compound. J. Biomol. Screen *12*, 938–945. https://doi.org/10.1177/1087057107306130.

Blackburn, E.H., and Collins, K. (2011). Telomerase: an RNP enzyme synthesizes DNA. Cold Spring Harb Perspect. Biol. *3*. https://doi.org/10.1101/cshperspect.a003558.

Blackburn, E.H., Epel, E.S., and Lin, J. (2015). Human telomere biology: a contributory and interactive factor in aging, disease risks, and protection. Science *350*, 1193–1198. https://doi.org/10.1126/science.aab3389.

Celeghin, A., Giunco, S., Freguja, R., Zangrossi, M., Nalio, S., Dolcetti, R., and De Rossi, A. (2016). Short-term inhibition of TERT induces telomere length-independent cell cycle arrest and apoptotic response in EBV-immortalized and transformed B cells. Cell Death Dis *7*, e2562. https://doi.org/10.1038/cddis.2016.425.

Chen, K.S., Lim, J.W.C., Richards, L.J., and Bunt, J. (2017). The convergent roles of the nuclear factor I transcription factors in development and cancer. Cancer Lett. *410*, 124–138. https://doi.org/10.1016/j.canlet.2017.09.015.

Cheng, S.H., Huang, T.T., Cheng, Y.H., Tan, T.B.K., Horng, C.F., Wang, Y.A., Brian, N.S., Shih, L.S., and Yu, B.L. (2017). Validation of the 18-gene classifier as a prognostic biomarker of distant metastasis in breast cancer. PLoS ONE *12*, e0184372. https://doi.org/10.1371/journal.pone.0184372.

Cox, J., and Mann, M. (2008). MaxQuant enables high peptide identification rates, individualized p.p.b.-range mass accuracies and proteome-wide protein quantification. Nat. Biotechnol. *26*, 1367–1372. https://doi.org/10.1038/nbt.1511.

Cui, J., Li, Y., Zhu, L., Liu, D., Songyang, Z., Wang, H.Y., and Wang, R.F. (2012). NLRP4 negatively regulates type I interferon signaling by targeting the kinase TBK1 for degradation via the ubiquitin ligase DTX4. Nat. Immunol. *13*, 387–395. https://doi.org/10.1038/ni.2239.

Doksani, Y., and de Lange, T. (2016). Telomere-internal double-strand breaks are repaired by homologous recombination and PARP1/Lig3-dependent end-joining. Cell Rep *17*, 1646–1656. https://doi.org/10.1016/j.celrep.2016.10.008.

Fornes, O., Castro-Mondragon, J.A., Khan, A., van der Lee, R., Zhang, X., Richmond, P.A., Modi, B.P., Correard, S., Gheorghe, M., Baranasic, D., et al. (2020). Jaspar 2020: update of the open-access database of transcription factor binding profiles. Nucleic Acids Res. *48*, D87–D92. https://doi.org/10.1093/nar/gkz1001.

Gingras, A.C., Abe, K.T., and Raught, B. (2019). Getting to know the neighborhood: using proximity-dependent biotinylation to characterize protein complexes and map organelles. Curr. Opin. Chem. Biol. *48*, 44–54. https://doi.org/10.1016/j.cbpa.2018.10.017.

Giunco, S., Celeghin, A., Gianesin, K., Dolcetti, R., Indraccolo, S., and De Rossi, A. (2015). Cross talk between EBV and telomerase: the role of TERT and NOTCH2 in the switch of latent/lytic cycle of the virus. Cell Death Dis *6*, e1774. https://doi.org/10.1038/cddis.2015.145.

Goueli, B.S., and Janknecht, R. (2004). Upregulation of the catalytic telomerase subunit by the transcription factor ER81 and oncogenic HER2/Neu, Ras, or Raf. Mol. Cell Biol *24*, 25–35. https://doi.org/10.1128/mcb.24.1.25-35.2004.

Gronostajski, R.M. (2000). Roles of the NFI/CTF gene family in transcription and development. Gene *249*, 31–45. https://doi.org/10.1016/s0378-1119(00)00140-2.

Groth, C., Alvord, W.G., Quinones, O.A., and Fortini, M.E. (2010). Pharmacological analysis of Drosophila melanogaster gamma-secretase with respect to differential proteolysis of Notch and APP. Mol. Pharmacol. *77*, 567–574. https://doi.org/10.1124/mol.109.062471.

Guterres, A.N., and Villanueva, J. (2020). Targeting telomerase for cancer therapy. Oncogene *39*, 5811–5824. https://doi.org/10.1038/s41388-020-01405-w.

Harley, C.B., Futcher, A.B., and Greider, C.W. (1990). Telomeres shorten during ageing of human fibroblasts. Nature *345*, 458–460. https://doi.org/10.1038/345458a0.

Harvey, A., Mielke, N., Grimstead, J.W., Jones, R.E., Nguyen, T., Mueller, M., Baird, D.M., and Hendrickson, E.A. (2018). PARP1 is required for preserving telomeric integrity but is dispensable for A-NHEJ. Oncotarget *9*, 34821–34837. https://doi.org/10.18632/oncotarget.26201.

Hayashi, M.T., Cesare, A.J., Rivera, T., and Karlseder, J. (2015). Cell death during crisis is mediated by mitotic telomere deprotection. Nature *522*, 492–496. https://doi.org/10.1038/nature14513.

Hellman, L.M., and Fried, M.G. (2007). Electrophoretic mobility shift assay (EMSA) for detecting protein-nucleic acid interactions. Nat. Protoc. *2*, 1849–1861. https://doi.org/10.1038/nprot.2007.249.

Higashi, K., Hazama, S., Araki, A., Yoshimura, K., Iizuka, N., Yoshino, S., Noma, T., and Oka, M. (2014). A novel cancer vaccine strategy with combined IL-18 and HSV-TK gene therapy driven by the hTERT promoter in a murine colorectal cancer model. Int. J. Oncol. *45*, 1412–1420. https://doi.org/10.3892/ijo.2014.2557.

Hori, K., Fostier, M., Ito, M., Fuwa, T.J., Go, M.J., Okano, H., Baron, M., and Matsuno, K. (2004). Drosophila deltex mediates suppressor of Hairless-independent and late-endosomal activation of Notch signaling. Development *131*, 5527–5537. https://doi.org/10.1242/dev.01448.

Hornbeck, P.V., Zhang, B., Murray, B., Kornhauser, J.M., Latham, V., and Skrzypek, E. (2015). PhosphoSitePlus, 2014: mutations, PTMs and recalibrations. Nucleic Acids Res *43*, D512–D520. https://doi.org/10.1093/nar/gku1267.

Jiang, S., Tang, M., Xin, H., and Huang, J. (2017). Assessing telomerase activities in mammalian cells using the quantitative PCR-based telomeric repeat amplification Protocol (qTRAP). In Telomeres and Telomerase: Methods and Protocols, Z. Songyang, ed. (Springer New York), pp. 95–101. https://doi.org/10.1007/978-1-4939-6892-3_9.

Kim, D.I., Jensen, S.C., Noble, K.A., Kc, B., Roux, K.H., Motamedchaboki, K., and Roux, K.J. (2016). An improved smaller biotin ligase for BioID proximity labeling. Mol. Biol. Cell *27*, 1188–1196. https://doi.org/10.1091/mbc.E15-12-0844.

Kim, H., Li, F., He, Q., Deng, T., Xu, J., Jin, F., Coarfa, C., Putluri, N., Liu, D., and Songyang, Z. (2017). Systematic analysis of human telomeric dysfunction using inducible telosome/shelterin CRISPR/Cas9 knockout cells. Cell Discov *3*, 17034. https://doi.org/10.1038/celldisc.2017.34.

Li, W., Xu, H., Xiao, T., Cong, L., Love, M.I., Zhang, F., Irizarry, R.A., Liu, J.S., Brown, M., and Liu, X.S. (2014). MAGeCK enables robust identification of essential genes from genome-scale CRISPR/Cas9 knockout screens. Genome Biol. *15*, 554. https://doi.org/10.1186/s13059-014-0554-4.

Lin, J.R., and Hu, J. (2013). SeqNLS: nuclear localization signal prediction based on frequent pattern mining and linear motif scoring. PLoS ONE *8*, e76864. https://doi.org/10.1371/journal.pone.0076864.

Liu, D. (2011). Analysis of average telomere length in cultured human cells. Methods Mol. Biol. *735*, 13–19. https://doi.org/10.1007/978-1-61779-092-8_2.

Liu, F., Feng, X., and Ma, W. (2017). Analysis of telomere proteins by chromatin immunoprecipitation (ChIP). Methods Mol. Biol. *1587*, 205–214. https://doi.org/10.1007/978-1-4939-6892-3_19.

Liu, Y., Liu, F., Cao, Y., Xu, H., Wu, Y., Wu, S., Liu, D., Zhao, Y., Songyang, Z., and Ma, W. (2018). Shwachman-diamond syndrome protein SBDS maintains human telomeres by regulating telomerase recruitment. Cell Rep *22*, 1849–1860. https://doi.org/10.1016/j.celrep.2018.01.057.

Luo, D., de Morree, A., Boutet, S., Quach, N., Natu, V., Rustagi, A., and Rando, T.A. (2017). Deltex2 represses MyoD expression and inhibits myogenic differentiation by acting as a negative regulator of Jmjd1c. Proc. Natl. Acad. Sci. U S A *114*, E3071–E3080. https://doi.org/10.1073/pnas.1613592114.

Luo, Y., Yi, Y., and Yao, Z. (2009). Growth arrest in ovarian cancer cells by hTERT inhibition short-hairpin RNA targeting human telomerase reverse transcriptase induces immediate growth inhibition but not necessarily induces apoptosis in ovarian cancer cells. Cancer Invest *27*, 960–970. https://doi.org/10.3109/07357900802491451.

Ma, J., Chen, T., Wu, S., Yang, C., Bai, M., Shu, K., Li, K., Zhang, G., Jin, Z., He, F., et al. (2019). iProX: an integrated proteome resource. Nucleic Acids Res. *47*, D1211–D1217. https://doi.org/10.1093/nar/gky869.

Macfarlan, T., Kutney, S., Altman, B., Montross, R., Yu, J., and Chakravarti, D. (2005). Human THAP7 is a chromatin-associated, histone tail-binding protein that represses transcription via recruitment of HDAC3 and nuclear hormone receptor corepressor. J. Biol. Chem. *280*, 7346–7358. https://doi.org/10.1074/jbc.M411675200.

Maciejowski, J., and de Lange, T. (2017). Telomeres in cancer: tumour suppression and genome instability. Nat. Rev. Mol. Cell Biol *18*, 175–186. https://doi.org/10.1038/nrm.2016.171.

Marchler-Bauer, A., Bo, Y., Han, L., He, J., Lanczycki, C.J., Lu, S., Chitsaz, F., Derbyshire, M.K., Geer, R.C., Gonzales, N.R., et al. (2017). CDD/SPARCLE: functional classification of proteins via subfamily domain architectures. Nucleic Acids Res. *45*, D200–D203. https://doi.org/10.1093/nar/gkw1129.

Matsuno, K., Eastman, D., Mitsiades, T., Quinn, A.M., Carcanciu, M.L., Ordentlich, P., Kadesch, T., and Artavanis-Tsakonas, S. (1998). Human deltex is a conserved regulator of Notch signalling. Nat.

Genet. *19*, 74–78. https://doi.org/10.1038/ng0598-74.

Mukhopadhyay, S.S., Wyszomierski, S.L., Gronostajski, R.M., and Rosen, J.M. (2001). Differential interactions of specific nuclear factor I isoforms with the glucocorticoid receptor and STAT5 in the cooperative regulation of WAP gene transcription. Mol. Cell Biol *21*, 6859–6869. https://doi.org/10.1128/MCB.21.20.6859-6869.2001.

Norrman, K., Fischer, Y., Bonnamy, B., Wolfhagen Sand, F., Ravassard, P., and Semb, H. (2010). Quantitative comparison of constitutive promoters in human ES cells. PLoS ONE *5*, e12413. https://doi.org/10.1371/journal.pone.0012413.

Pathan, M., Keerthikumar, S., Ang, C.S., Gangoda, L., Quek, C.Y., Williamson, N.A., Mouradov, D., Sieber, O.M., Simpson, R.J., Salim, A., et al. (2015). FunRich: an open access standalone functional enrichment and interaction network analysis tool. Proteomics *15*, 2597–2601. https://doi.org/10.1002/pmic.201400515.

Ramlee, M.K., Wang, J., Toh, W.X., and Li, S. (2016). Transcription regulation of the human telomerase reverse transcriptase (hTERT) gene. Genes (Basel) *7*. https://doi.org/10.3390/genes7080050.

Roake, C.M., and Artandi, S.E. (2020). Regulation of human telomerase in homeostasis and disease. Nat. Rev. Mol. Cell Biol *21*, 384–397. https://doi.org/10.1038/s41580-020-0234-z.

Saretzki, G., Sitte, N., Merkel, U., Wurm, R.E., and von Zglinicki, T. (1999). Telomere shortening triggers a p53-dependent cell cycle arrest via accumulation of G-rich single stranded DNA fragments. Oncogene *18*, 5148–5158. https://doi.org/10.1038/sj.onc.1202898.

Schultz, J., Copley, R.R., Doerks, T., Ponting, C.P., and Bork, P. (2000). SMART: a web-based tool for the study of genetically mobile domains. Nucleic Acids Res. *28*, 231–234. https://doi.org/10.1093/nar/28.1.231.

Shay, J.W. (2013). Are short telomeres predictive of advanced cancer? Cancer Discov. *3*, 1096–1098. https://doi.org/10.1158/2159-8290.CD-13-0506.

Shay, J.W. (2016). Role of telomeres and telomerase in aging and cancer. Cancer Discov. *6*, 584–593. https://doi.org/10.1158/2159-8290.CD-16-0062.

Takeyama, K., Aguiar, R.C., Gu, L., He, C., Freeman, G.J., Kutok, J.L., Aster, J.C., and Shipp, M.A. (2003). The BAL-binding protein BBAP and related Deltex family members exhibit ubiquitin-protein isopeptide ligase activity. J. Biol. Chem. *278*, 21930–21937. https://doi.org/10.1074/jbc.M301157200.

Tang, Z., Li, C., Kang, B., Gao, G., Li, C., and Zhang, Z. (2017). GEPIA: a web server for cancer and normal gene expression profiling and interactive analyses. Nucleic Acids Res. *45*, W98–W102. https://doi.org/10.1093/nar/gkx247.

Thierbach, R., and Steinberg, P. (2009). Automated soft agar assay for the high-throughput screening of anticancer compounds. Anal Biochem. *387*, 318–320. https://doi.org/10.1016/j.ab.2009.01.029.

Thul, P.J., and Lindskog, C. (2018). The human protein atlas: a spatial map of the human proteome. Protein Sci. *27*, 233–244. https://doi.org/10.1002/pro.3307.

Victorelli, S., and Passos, J.F. (2017). Telomeres and cell senescence - size matters not. EBioMedicine *21*, 14–20. https://doi.org/10.1016/j.ebiom.2017.03.027.

Wang, G., Gao, Y., Li, L., Jin, G., Cai, Z., Chao, J.I., and Lin, H.K. (2012). K63-linked ubiquitination in kinase activation and cancer. Front Oncol. *2*, 5. https://doi.org/10.3389/fonc.2012.00005.

Wang, S., Zhao, Y., Hu, C., and Zhu, J. (2009). Differential repression of human and mouse TERT genes during cell differentiation. Nucleic Acids Res. *37*, 2618–2629. https://doi.org/10.1093/nar/gkp125.

Wang, S., and Zhu, J. (2003). Evidence for a relief of repression mechanism for activation of the human telomerase reverse transcriptase promoter. J. Biol. Chem. *278*, 18842–18850. https://doi.org/10.1074/jbc.M209544200.

Wang, T., Wei, J.J., Sabatini, D.M., and Lander, E.S. (2014). Genetic screens in human cells using the CRISPR-Cas9 system. Science *343*, 80–84. https://doi.org/10.1126/science.1246981.

Wang, Y., Susac, L., and Feigon, J. (2019). Structural biology of telomerase. Cold Spring Harb Perspect. Biol. *11*. https://doi.org/10.1101/cshperspect.a032383.

Weinrich, S.L., Pruzan, R., Ma, L., Ouellette, M., Tesmer, V.M., Holt, S.E., Bodnar, A.G., Lichtsteiner, S., Kim, N.W., Trager, J.B., et al. (1997). Reconstitution of human telomerase with the template RNA component hTR and the catalytic protein subunit hTRT. Nat. Genet. *17*, 498–502. https://doi.org/10.1038/ng1297-498.

Wright, W.E., Pereira-Smith, O.M., and Shay, J.W. (1989). Reversible cellular senescence: implications for immortalization of normal human diploid fibroblasts. Mol. Cell Biol *9*, 3088–3092.

Zenker, M., Bunt, J., Schanze, I., Schanze, D., Piper, M., Priolo, M., Gerkes, E.H., Gronostajski, R.M., Richards, L.J., Vogt, J., et al. (2019). Variants in nuclear factor I genes influence growth and development. Am. J. Med. Genet. C Semin. Med. Genet. *181*, 611–626. https://doi.org/10.1002/ajmg.c.31747.

Zhang, F., Cheng, D., Wang, S., and Zhu, J. (2016). Human specific regulation of the telomerase reverse transcriptase gene. Genes (Basel) *7*. https://doi.org/10.3390/genes7070030.

Zhang, P., Yang, Y., Nolo, R., Zweidler-McKay, P.A., and Hughes, D.P. (2010). Regulation of NOTCH signaling by reciprocal inhibition of HES1 and Deltex 1 and its role in osteosarcoma invasiveness. Oncogene *29*, 2916–2926. https://doi.org/10.1038/onc.2010.62.

Zhang, X., Mar, V., Zhou, W., Harrington, L., and Robinson, M.O. (1999). Telomere shortening and apoptosis in telomerase-inhibited human tumor cells. Genes Dev. *13*, 2388–2399. https://doi.org/10.1101/gad.13.18.2388.

Zheng, Y., Liu, Q., Wu, Y., Ma, L., Zhang, Z., Liu, T., Jin, S., She, Y., Li, Y.P., and Cui, J. (2018). Zika virus elicits inflammation to evade antiviral response by cleaving cGAS via NS1-caspase-1 axis. EMBO J. *37*. https://doi.org/10.15252/embj.201899347.

Zhou, Q., Liu, M., Xia, X., Gong, T., Feng, J., Liu, W., Liu, Y., Zhen, B., Wang, Y., Ding, C., and Qin, J. (2017). A mouse tissue transcription factor atlas. Nat Commun. *8*, 15089. https://doi.org/10.1038/ncomms15089.

Zhou, Z., Li, M., Zhang, L., Zhao, H., Sahin, O., Chen, J., Zhao, J.J., Songyang, Z., and Yu, D. (2018). Oncogenic kinase-induced PKM2 tyrosine 105 phosphorylation converts Nononcogenic PKM2 to a tumor promoter and induces cancer stem-like cells. Cancer Res. *78*, 2248–2261. https://doi.org/10.1158/0008-5472.CAN-17-2726.

Zhu, J., Zhao, Y., and Wang, S. (2010). Chromatin and epigenetic regulation of the telomerase reverse transcriptase gene. Protein Cell *1*, 22–32. https://doi.org/10.1007/s13238-010-0014-1.

Zweifel, M.E., Leahy, D.J., and Barrick, D. (2005). Structure and Notch receptor binding of the tandem WWE domain of Deltex. Structure *13*, 1599–1611. https://doi.org/10.1016/j.str.2005.07.015.

STAR★METHODS

KEY RESOURCE TABLE

REAGENT or RESOURCE	SOURCE	IDENTIFIER
Antibodies		
Flag mouse mAb	Abmart	Cat# M20008, RRID:AB_2713960
β-actin rabbit mAb	ABclonal	Cat# AC004, RRID:AB_2737399
GAPDH mouse mAb	Abmart	Cat# M20006, RRID:AB_2737054
α-tubulin mouse mAb	Sigma	Cat# T5168, RRID:AB_477579
NFIC rabbit pAb	Cell Signaling Technology	Cat# 11911, RRID:AB_2797765
HA mouse mAb (IF, WB)	Sigma	Cat# H9658, RRID: AB_260092
HA rabbit pAb (WB)	Sigma	Cat# H6908, RRID:AB_260070
HA rabbit mAb (EMSA, ChIP)	Cell Signaling Technology	Cat# 3724, RRID:AB_1549585
Lamin A/C mouse mAb	Sigma	Cat# SAB4200236, RRID:AB_10743057
Histone H3 rabbit pAb	Abcam	Cat# ab1791, RRID:AB_302613
Myc mouse mAb	Sigma	Cat# M4439, RRID:AB_439694
Rabbit IgG	Millipore	Cat# PP64, RRID:AB_97852
H3K4me3 rabbit mAb	Cell Signaling Technology	Cat#9751, RRID:AB_2616028
H3K9me3 rabbit pAb	Abcam	Cat# ab8898, RRID:AB_306848
H3K27me3 rabbit pAb	Active Motif	Cat# 39155, RRID:AB_2561020
PolII CTD-pS2 rat mAb	Active Motif	Cat# 61083, RRID:AB_2687450
Donkey Anti-Rabbit IgG (Alexa Fluor 488)	Thermo Fisher Scientific	Cat# A-21206, RRID:AB_2535792
Donkey anti-Mouse IgG (Alexa Fluor 555)	Thermo Fisher Scientific	Cat# A-31570, RRID:AB_2536180
IRDye 800CW Goat anti-Rabbit IgG	LI-COR Biosciences	Cat# 926-32211, RRID:AB_621843
IRDye 680RD Goat anti-Mouse IgG	LI-COR Biosciences	Cat# 926-68070, RRID:AB_10956588
Chemicals, peptides, and recombinant proteins		
Dibenzazepine	Selleckchem	Cat# S2711
MTT [3-(4,5-dimethylthiazol-2-yl)-2,5-diphenyltetrazolium bromide]	Sigma	Cat# V900888
Critical commercial assays		
RNAiso Plus	TAKARA	Cat# 9109
EZ-press RNA Purification Kit	EZBioscience	Cat# B0004D
PrimeScript™ RT reagent Kit with gDNA Eraser	TAKARA	Cat# RR047
2×RealStar Green Fast Mixture (qTRAP)	GenStar	Cat# A301
ChamQ Universal SYBR qPCR Master Mix (qPCR)	Vazyme	Cat# Q711-02
Cell Counting Kit-8 (CCK-8)	Bimake	B34304
AxyPrep Blood Genomic DNA Miniprep Kit	Axygen	Cat# AP-MN-BL-GDNA
Dual-Luciferase® Reporter Assay System	Promega	Cat# E1910
Chemiluminescent Nucleic Acid Detection Module	Thermo Fisher Scientific	Cat# 89880
Streptavidin Magnetic Beads	Thermo Fisher Scientific	Cat# 88817
Protein A/G Magnetic Beads	Bimake	Cat# B23201
Anti-Myc magnetic beads	Bimake	B26301
Glutathione Sepharose® 4B	Merck	GE17-0756-01
Deposited data		
TERT CRISPR/Cas9 screen data analysis	This paper	PRJNA694462
DTX2 BioID MS data analysis	This paper	PXD023795

(*Continued on next page*)

Continued

REAGENT or RESOURCE	SOURCE	IDENTIFIER
Mendeley dataset: unprocessed images	This paper	https://10.17632/jty4n5rd6y.1
Experimental models: Cell lines		
HEK293T	ATCC	N/A
HeLa	ATCC	N/A
HT-1080	ATCC	N/A
Hs578T	ATCC	N/A
MDA-MB-231	ATCC	N/A
MCF7	ATCC	N/A
DLD1	ATCC	N/A
Oligonucleotides: see Table S4		
Software and algorithms		
GraphPad Prism 7.00	N/A	https://www.graphpad.com/
DOG 2.0	N/A	http://dog.biocuckoo.org/
MAGeCK analysis	N/A	(Li et al., 2014)
ImageQuant 5.2	N/A	https://imagequanttl.software.informer.com/
Maxquant 1.6.2.10	N/A	https://www.maxquant.org/
FunRich 3.1.3	N/A	http://www.funrich.org/

RESOURCE AVAILABILITY

Lead contact

Further information and requests for resources and reagents should be directed to and will be fulfilled by the Lead Contact, Zhou Songyang (songyanz@mail.sysu.edu.cn).

Materials availability

The knockout cell lines and plasmids generated in this study are available from the Lead Contact without restriction.

Data and code availability

- The high-throughput sequencing data of CRISPR/Cas9 screen for hTERT transcription regulators have been uploaded to SRA database with accession PRJNA694462. The mass spectrometry proteomics data have been deposited to the ProteomeXchange Consortium with accession PXD023795. All unprocessed images have been deposited at Mendeley Data (https://10.17632/jty4n5rd6y.1) and are publicly available as of the date of publication.
- This paper does not report original code.
- Any additional information required to reanalyze the data reported in this paper is available from the lead contact upon request.

EXPERIMENTAL MODEL AND SUBJECT DETAILS

Cell lines and cell culture

Cell lines HEK293T (human embryonic kidney), HeLa (cervical cancer), HT-1080 (fibrosarcoma), DLD1 (colorectal adenocarcinoma), Hs578T and MDA-MB-231 (breast adenocarcinoma) were purchased from ATCC. DLD1 cells were cultured in RPMI1640 (Gibco, 11,875-093) supplemented with 10% FBS (Excell biotech, FSP500). Other cells were cultured in DMEM (Corning; 10-013-CVR) supplemented with 10% FBS. All cell lines were confirmed to be free of mycoplasma contamination.

METHOD DETAILS

CRISPR/Cas9-mediated inducible knockout screen

An EF1α promoter-driven EGFP expression lentiviral vector (EF1α-EGFP) served as screening control. The *hTERT* core promoter (the region spanning the *hTERT* translation start site (TSS) and 454 bp upstream of it) (Higashi et al., 2014) was amplified using genomic DNA from HeLa cells to replace the EF1α promoter upstream of EGFP (hTERT-EGFP). HeLa or HEK293T cells were first transduced with lentiviruses encoding doxycycline (Dox)-inducible Cas9 (iCas9) (Kim et al., 2017) and selected with G418 (250 μg/mL) for 10 days. A clonal derivate for each cell line isolated by limiting dilution cloning and confirmed to have moderate iCas9 expression upon induction was used for all subsequent experiments described in this study. The HeLa-iCas9 line was used for the KO screen and subsequently transduced with either hTERT-EGFP or EF1α-EGFP lentiviruses and selected with puromycin (2 μg/mL) for 3 days. GFP-positive cells that were further enriched by FACS were used as reporter cell lines.

Two sgRNA libraries (Addgene, 51,047 & 51,043) were packaged as lentiviruses, which were transduced separately into the reporter cell lines at low MOI (~0.3) with ≥100-fold coverage. Infected cells were selected with blasticidin (10 μg/mL) for 5 days. A portion of the cells were cultured without Dox and collected as the basal group. Cells that were cultured in Dox (1 μg/mL) for 7 days went through two rounds of FACS sorting for GFP-negative cells (sorted group).

High-throughput sequencing and data analysis

Genomic DNA was extracted from both basal and sorted groups for barcode amplification of the integrated sgRNAs for high-throughput sequencing (Novogene) (see Table S4 for barcodes). Sequencing data were first segregated into each sample group based on individual barcodes. Only sgRNAs that perfectly matched reference sequences from the sgRNA libraries were counted. Only sgRNAs that satisfied the following two conditions were considered as enriched, their fold change of reads in the hTERT-EGFP sorted group was ≥2-fold over its basal group, and their fold change of reads (sorted over basal) in hTERT-EGFP cells was more than their change in EF1α-EGFP cells. We also performed MAGeCK analysis (Li et al., 2014) using the sgRNA reads of sorted and basal groups from both hTERT-EGFP and EF1α-EGFP samples to identify significantly enriched genes. The corresponding genes with $p < 0.05$ were assigned as enriched genes. Genes with $p < 0.01$ and at least two sgRNAs significantly enriched were chosen as candidates. The high-throughput sequencing data have been deposited to the NCBI BioProject database, and is available at https://dataview.ncbi.nlm.nih.gov/object/PRJNA694462?reviewer=pi472nb79brvtoe17tbhcle6fq.

Generation of KO lines using dual-sgRNA strategies

For preliminary analysis, pooled KO cells were generated using two sgRNAs targeting non-overlapping regions for each candidate gene. The sgRNAs were cloned into the LentiGuide vector with the hygromycin or blasticidin selection marker (Kim et al., 2017). Lentiviruses encoding the sgRNAs were then packaged and transduced into iCas9-expressing HEK293T or HeLa cells. Gene knockout was induced by culturing the cells in Dox (1 μg/mL) for 48 h. For each targeted allele, this dual-sgRNA strategy may result in indels (at one or both sgRNA target sites) and/or deletions (precise or imprecise) of the intervening sequences between the two sgRNA target sites.

To generate clonal KO cells, two sgRNAs targeting different exons of the same gene were cloned into px458-based (Addgene, 134,449) vectors expressing Cas9-EGFP or Cas9-mScarlet and transfected into HeLa cells using Lipofectamine 3,000 (Thermo Fisher Scientific; L3000015). EGFP and mScarlet double-positive cells were sorted by FACS and seeded into 96-well plates 48 h after transfection for clonal isolation. For KO verification, the genomic region encompassing the intervening sequences between the two sgRNA targeting sites was amplified and ligated into pEASY-Blunt Zero vectors (Transgen, CB501) for Sanger sequencing.

RNA extraction and real-time qPCR

Total RNA was extracted using RNAiso Plus (TAKARA, 9109) or the EZ-press RNA Purification Kit (EZBioscience, B0004D) and reverse transcribed with the PrimeScript RT reagent Kit with gDNA Eraser (TAKARA, RR047). To quantify gene expression, real-time PCR was conducted using the ChamQ Universal SYBR qPCR Master Mix (Vazyme, Q711-03) on a LightCycler 480II real-time PCR system (Roche). The relative level of mRNA was quantified by $2^{-\Delta\Delta Ct}$ normalized to GAPDH and control group.

Detection of relative telomerase activity (qTRAP)

The qTRAP (quantitative Telomere Repeat Amplification Protocol) assay was performed as previously described (Jiang et al., 2017). Briefly, diluted cell lysate (10-100 cells/μL) was used in 10 μL reaction mix containing 50 ng of TS and ACX primers, 1 mM EGTA, and the qPCR Supermix (GenStar, A301). Serially diluted telomerase-positive control samples were used to derive a standard curve based on which relative telomerase activities of test samples were calculated.

Analysis of average telomere length

Average telomere length was analyzed using the Telomere Restriction Fragment (TRF) assay (Liu, 2011). Briefly, cells were collected at different times points for genomic DNA extraction (Axygen, AP-MN-BL-GDNA) and restriction enzyme digestion (*Hin*fI, *Rsa*I, and *Msp*I). Following agarose gel electrophoresis and gel drying, the gel was hybridized to γ-^{32}P-labeled telomere DNA probes $(TTAGGG)_3$ and quantified on the GE Typhoon FLA 9000 Gel Imaging Scanner. ImageQuant 5.2 was used to calculate average telomere length.

CCK-8 assay

Various cell lines were infected with lentiviruses encoding *DTX2* or *hTERT* shRNAs (see Table S4 for shRNA sequences). At 72 h after infection, cells were seeded in 96-well plates (at 1,500 cells/well in 6 plates). Cell viability was determined daily using the Cell Counting Kit-8 (Bimake, B34304) and by measuring OD450 absorbance on a Biotek plate reader.

Cell apoptosis detection

Cells were collected one week after transduction with viruses encoding *DTX2* or *hTERT* shRNAs, and then stained with Annexin V-FITC and PI following the instructions of the TransDetect Annexin V-FITC/PI Cell Apoptosis Detection Kit (TransGen, FA101). Fluorescence signals were detected using the Beckman CytoFLEX Flow Cytometer. Annexin V^+/PI^- and Annexin V^+/PI^+ populations were defined respectively as early and late apoptotic cells.

Soft agar assay

2×DMEM supplemented with 20% FBS and 2×antibiotics were mixed with 1.2% or 0.7% Noble agar solution (1:1 ratio) to generate 0.6% or 0.35% agar/medium mix, respectively. 0.5 mL of 0.6% agar/medium mix were added to each well of 24-well plate and solidified for 1 hour. 5,000 or 10,000 cells were resuspended in 0.5 mL of 0.35% agar/medium and seeded in each well. Incubate plates at 37°C in humidified incubator for 10 to 20 days. Feed cells two times per week with cell culture medium. Stain live colonies by adding 100 μL of 5 mg/mL MTT [3-(4,5-dimethylthiazol-2-yl)-2,5-diphenyltetrazolium bromide] and incubate for 2 h. Images were captured with camera.

Immunostaining and confocal microscopy

Imaging analysis was carried out as described previously (Liu et al., 2018). Briefly, cells seeded on glass slides were fixed in 4% paraformaldehyde, permeabilized with 0.5% TritonX-100, and incubated with appropriate primary and secondary antibodies (see key resource table). The nucleus was stained with Hoechst 33,342 (1 μg/mL). Cells were visualized under a confocal laser scanning microscope (Leica TCS SP5).

Cell fractionation

Cell fractionation was carried out as previously described (Zhou et al., 2018). All steps were carried out at 4°C with protease inhibitors added to all solutions. Briefly, cells were incubated in hypotonic buffer (10 mM HEPES, pH 8.0; 1.5 mM $MgCl_2$; 10 mM KCl) for 15 min and centrifuged at 2,000 *g* for 5 min. The pellet was incubated in cytosol lysis buffer (hypotonic buffer plus 0.5% NP-40) for 30 min and centrifuged at 13,000 *g* for 10 min. The supernatant was collected as the cytosol fraction. The pellet was washed in hypotonic buffer twice and lysed in nucleus lysis buffer (10 mM HEPES, pH 8.0; 1.5 mM $MgCl_2$; 400 mM NaCl; 0.1 mM EDTA; 20% glycerol). The nuclear lysate was sonicated at 30% Ampl for 10 cycles of 2 s on and 8 s off, and centrifuged at 13,000 *g* for 15 min. The supernatant was collected as the nuclear fraction.

Chromatin association assay

This assay was performed as previously described (Macfarlan et al., 2005). Briefly, ~10^7 cells were resuspended in NIB buffer (15 mM Tris-HCl, pH 7.4; 60 mM KCl; 15 mM $MgCl_2$; 15 mM NaCl; 1 mM $CaCl_2$)

plus 0.3% NP-40 and centrifuged at 600 *g* for 3 min. The supernatant was collected as the cytosolic extraction. The nuclei were washed with NIB buffer plus 0.6% NP-40 and centrifuged again at 600 *g* for 3 min, with the supernatant designated as Wash 1. The nuclei were treated with micrococcal nuclease (Thermo, EN0181) in NIB buffer for 8 min at 37°C and then centrifuged at 12,000 *g* for 10 min. This supernatant was designated as Wash 2 and the pellet was centrifuged in 2 mM EDTA (pH 8.0) at 12,000 *g* for 10 min, with the supernatant and pellet retained as soluble and insoluble chromatin fractions respectively. The presence of nucleosomes in chromatin fractions was verified by DNA electrophoresis. All fractions were subjected to SDS-PAGE and immunoblot analysis with the appropriate antibodies (see key resource table).

Chromatin immunoprecipitation (ChIP)

ChIP assays were performed as previously described (Liu et al., 2017). Briefly, ~10^7 cells were fixed with 1% formaldehyde and quenched with 125 mM glycine for 15 min. Cells were pelleted and washed sequentially with Solution A (10 mM HEPES pH 7.9, 1 mM EDTA, 0.5 mM EGTA, 0.25% Triton X-100) and Solution B (10 mM HEPES pH 7.9, 1mM EDTA, 0.5 mM EGTA, 200 mM NaCl) before being lysed in Solution C (0.1% sodium deoxycholate, 150 mM NaCl, 50 mM HEPES pH 7.5, 0.1% SDS, 1% Triton X-100). The lysate was sonicated for 50 cycles of 30 s on and 30 s off (Bioruptor Pico) to ensure DNA fragmented to <1,000 bp. For each ChIP, 100 μL of clarified chromatin was incubated with indicated antibodies and then protein A/G magnetic beads (Bimake, B23202). Eluted chromatin DNA was ultimately purified using the QIAquick PCR purification kit (Qiagen, 28,106) for qPCR analysis (see Table S4 for primer sequences).

BioID-mediated proximity-labeling and MS analysis

BioID-mediated proximity labeling was carried out as described (Kim et al., 2016) with minor modifications. BioID was fused to the N-terminus of full-length DTX2 and cloned into a Flag-HA-tagging lentiviral vector for expression in HeLa DTX2 KO cells. About 4×10^7 cells were cultured in media containing 50 μM biotin for 16 h before being collected for lysis in 3 mL of RIPA buffer (10 mM Tris-Cl, pH 7.4; 140 mM NaCl; 0.1% SDS; 1 mM EDTA; 0.5 mM EGTA; 0.1% sodium deoxycholate; 1% Triton X-100; 1× protease and phosphatase inhibitors cocktail). The lysate was sonicated at 30% Ampl for 30 cycles of 2 s on and 8 s off (Sonics Vibra-Cell; VCX130PB) and centrifuged at 13,000 *g* for 10 min at 4°C. The supernatant was then incubated with Streptavidin magnetic beads (Thermo, 88,816) with rotation for 2 h at 4°C. The washed beads were then prepared for mass spectrometry (Wininnovate Bio Company) on Triple TOF 6600 (SCIEX, Concord, ON, Canada).

Mass spectrometry data were collected using the information-dependent analysis (IDA) mode. The LS-MS/MS raw data (in triplicates) were processed with the Maxquant software (Cox and Mann, 2008) for peptide search using the human proteome dataset (Swiss-Prot) (downloaded from UniProt on Oct 30, 2018). The mass spectrometry proteomics data have been deposited to the ProteomeXchange Consortium (http://proteomecentral.proteomexchange.org) via the iProX partner repository (Ma et al., 2019) with the dataset identifier PXD023795.

Contaminates as well as proteins that appeared in only one replicate were excluded. The iBAQ (Intensity Based Absolute Quantification) value of each protein from MS data was calculated using the Maxquant software and normalized to total iBAQs in each sample to generate the fraction of total (FOT) value (Zhou et al., 2017). Proteins whose FOT values in the BioID-DTX2 group were ≥3-fold over those in the control group were designated as proximal candidates.

Dual luciferase reporter assay

The genomic region from −178 to +65 relative to the transcription start site of human *HES1* (core promoter) (Luo et al., 2017) was amplified using HEK293T genomic DNA and designated as HES1P wt. To block Notch activation, the RBP-J binding site GTGGGAA in the *HES1* core promoter was mutated to GTGAAAA (Luo et al., 2017) and designated as HES1P mut. These sequences were respectively cloned into pGL4.10 (Promega, E6651) to drive firefly luciferase expression. An SV40 promoter-driven Renilla luciferase vector (pRL-SV40, Promega, E2231) served as an internal control. Expression plasmids and pRL-SV40 were co-transfected with pGL4.10-HES1P wt or pGL4.10-HES1P mut into HEK293T cells. The cells were then harvested 24 h after transfection for analysis using the Dual-Luciferase Reporter Assay System (Promega; E1910) following manufacturer's instructions.

Co-immunoprecipitation (co-IP)

HEK293T cells were transiently transfected with expression plasmids using Polyethylenimine (Polyscience, 23,966). At 24 h after transfection, cells were lysed with NETN buffer and sonicated at 30% Ampl for 5 cycles

of 2 s on and 8 s off (Sonics Vibra-Cell; VCX130PB). Clear lysate was incubated with indicated antibodies for 2-4 h and protein A/G magnetic beads for 1 hour. The beads were washed with NETN buffer for 6 times and the precipitates were analyzed by immunoblotting with appropriate antibodies (see key resource table).

Electrophoretic mobility shift assay (EMSA)

EMSA was performed as described (Hellman and Fried, 2007) with minor modifications. Briefly, cells were collected 24 h after transfection and lysed in Buffer A (20 mM HEPES, pH 7.9; 10 mM NaCl; 1 mM $MgCl_2$; 0.15 mM spermine; 10% glycerol; 0.1 mM EDTA; 0.1 mM EGTA; 0.5 mM DTT). Annealed biotin-labeled dsDNA probes were added to lysate in Buffer W (20 mM HEPES, pH 7.9; 100 mM NaCl; 80 mM KCl; 10% glycerol; 1 mM $MgCl_2$; 0.15 mM spermine; 0.1 mM EDTA; 0.1 mM EGTA; 0.5 mM DTT) for reactions to occur. Whenever appropriate, rabbit IgG or an anti-HA rabbit mAb (CST, 3,724) was also added to the reaction. The DNA-protein complex was separated on a 5% non-denaturing PAGE gel, blotted onto nylon membranes (GE Healthcare, RPN303B), and detected using the Chemiluminescent Nucleic Acid Detection Module (Thermo, 89,880).

Ubiquitination assay

Ubiquitination assays were carried out as described (Zheng et al., 2018). HEK293T cells were transiently transfected with expression plasmids for 24 h. Cells were lysed in NETN buffer plus 0.05% SDS. The lysate was sonicated at 30% Ampl for 5 cycles of 2 s on and 8 s off (Sonics Vibra-Cell; VCX130PB) and then centrifuged at 12,000 *g* for 10 min at 4°C. About 1% of lysate was saved as input, and the rest was precipitated with Glutathione Sepharose 4B (GE Healthcare, 17-0756-01). The precipitates were analyzed by immunoblotting with appropriate antibodies (see key resource table).

QUANTIFICATION AND STATISTICAL ANALYSIS

All quantitative experiments were performed with at least three independent biological repeats unless otherwise indicated. The results were analyzed and graphed using the GraphPad Prism 7 software. All data are presented as mean ± SD Unpaired two-tailed Student's t test (two groups) or two-way ANOVA (multiple groups) was used to compare the mean of two or more samples, with p values and sample sizes indicated in the corresponding figure legends.